2017

Semiconductor Solid-Solution Nanostructures: Synthesis, Property Tailoring, and Applications

Baodan Liu
Shenyang National Laboratory for Materials Science

Jing Li
Shenyang National Laboratory for Materials Science

Wenjin Yang
Chinese Academy Of Sciences

Xinglai Zhang
Shenyang National Laboratory for Materials Science

Xin Jiang
Chinese Academy Of Sciences

See next page for additional authors

Publication Details

Liu, B., Li, J., Yang, W., Zhang, X., Jiang, X. & Bando, Y. (2017). Semiconductor Solid-Solution Nanostructures: Synthesis, Property Tailoring, and Applications. Small, 13 (45), 1701998-1-1701998-21.

Semiconductor Solid-Solution Nanostructures: Synthesis, Property Tailoring, and Applications

Abstract

The innovation of band-gap engineering in advanced materials caused by the alloying of different semiconductors into solid-solution nanostructures provides numerous opportunities and advantages in optoelectronic property tailoring. The semiconductor solid-solution nanostructures have multifarious emission wavelength, adjustability of absorption edge, tunable electrical resistivity, and cutting-edge photoredox capability, and these advantages can be rationalized by the assorted synthesis strategies such as, binary, ternary, and quaternary solid-solutions. In addition, the abundance of elements in groups IIB, IIIA, VA, VIA, and VIIA provides sufficient room to tailor-make the semiconductor solid-solution nanostructures with the desired properties. Recent progress of semiconductor solid-solution nanostructures including synthesis strategies, structure and composition design, band-gap engineering related to the optical and electrical properties, and their applications in different fields is comprehensively reviewed. The classification, formation principle, synthesis routes, and the advantage of semiconductor solid-solution nanostructures are systematically reviewed. Moreover, the challenges faced in this area and the future prospects are discussed. By combining the information together, it is strongly anticipated that this Review may shed new light on understanding semiconductor solid-solution nanostructures while expected to have continuous breakthroughs in band-gap engineering and advanced optoelectronic nanodevices.

Disciplines

Engineering | Physical Sciences and Mathematics

Publication Details

Liu, B., Li, J., Yang, W., Zhang, X., Jiang, X. & Bando, Y. (2017). Semiconductor Solid-Solution Nanostructures: Synthesis, Property Tailoring, and Applications. Small, 13 (45), 1701998-1-1701998-21.

Authors

Baodan Liu, Jing Li, Wenjin Yang, Xinglai Zhang, Xin Jiang, and Yoshio Bando

DOI: 10.1002/ ((please add manuscript number))

Semiconductor solid-solution nanostructures: synthesis, property tailoring and applications

Baodan Liu,[1,] Jing Li,[1] Wenjin Yang,[1] Xinglai Zhang,[1] Xin jiang[1] and Yoshio Bando[2]*

((This review paper is dedicated to my respected Ph.D supervisor, Prof. Yoshio Bando, on the auspicious occasion of his 70th birthday.))

Prof. B. D. Liu, Mr. J. Li, Mr. W. J. Yang, Dr. X. L. Zhang, Prof. X. Jiang
Shenyang National Laboratory for Materials Science, Institute of Metal Research, Chinese Academy of Sciences,
No. 72, Wenhua Road, Shenhe District, Shenyang, 110016, China
E-mail: baodanliu@hotmail.com
Prof. Y. Bando
World Premier International Center for Materials Nanoarchitectonics (WPI-MANA), National Institute for Materials Science (NIMS), Namiki 1-1, Tsukuba 305-0044, Japan
Australian Institute for Innovative Materials (AIM), University of Wollongong
Squires Way, North Wollongong, NSW 2500, Australia

Keywords: semiconductor, nanostructures, solid-solution, band-gap engineering, optoelectronic properties

Abstract

The innovation of band-gap engineering in advanced materials caused by the alloying of different semiconductors into solid solution nanostructures provides numerous opportunities and advantages in optoelectronic property tailoring. The semiconductor solid solutions nanostructures have multifarious emission wavelength, adjustability of absorption edge, tunable electrical resistivity and cutting-edge photo-redox capability, and these advantages can be rationalized by the assorted synthesis strategies such as, binary, ternary and quaternary solid solutions. In addition, the abundance of elements in groups IIB, IIIA, VA, VIA and VIIA provides sufficient room to tailor-made the semiconductor solid solution nanostructures having the desired properties. Herein, the recent progress of semiconductor solid solution nanostructures including synthesis strategies, structure and composition design, band-gap engineering related to the optical and electrical property, and their applications in different fields is comprehensively reviewed. The classification, formation principle, synthesis routes

and the advantage of semiconductor solid solutions nanostructures are systematically reviewed. Moreover, the challenges faced in this area and the future prospects are discussed. By combining the information together, we strongly anticipate that this review may shed new light on understanding semiconductor solid solution nanostructures while we are expecting continuous breakthroughs in the band-gap engineering and advanced opto-electronic nano-devices.

1. Introduction

Low-dimensional semiconductor nanostructures are considered to be promising candidates for the realization of high-performance and sensitive optoelectronic nanodevices, clean energy harvesting, photodegradation of organic pollutants and bio-related applications.[1-4] The suitability of the semiconductor nanostructure for above applications generally requires a careful consideration of its dimension, orientation, crystallinity, as well as the band-gap structures.[5] Especially, the band-gap of semiconductors is regarded as extremely important for a series of practical applications since the intrinsic physical properties such as optical absorption edge, emission wavelength and electrical conductivity are closely dependent on it. However, the available band gaps of natural semiconductors are very limited. It is quite challenging to search for appropriate intrinsic semiconductors satisfying the different and particular needs of the optoelectronic nanodevices and photocatalytic applications. Therefore, it is of great importance to develop facile and efficient strategy for the band-gap tailoring of semiconductor nanostructures to further promote their applications in diverse fields ranging from white light emitting diodes (LEDs), solar-cells, photodetectors, nanolasers, photocatalysis for H_2 production, and environmental processing, etc.

As an alternative and promising approach, the solid solution (doping or alloying) of semiconductors with proper elements or compounds has been demonstrated extremely efficient and useful in bulk semiconductors for effective band-gap engineering and optoelectronic property tailoring.[6, 7]For that reason, the selection of doped element or

compound is believed to be extremely important for expected properties since we can replace the anion or cation in host semiconductor and control their concentration for a tunable property. In this regard, specific synthesis strategy should be developed for the formation of solid solution and a precise control of the solubility, which directly affects the energy band structures, emission wavelength, absorption edge, and electrical transport.[8] Compared with the bulk films, semiconductor solid solution nanostructures have more advantages, such as large specific surface area, quantum confinement effect, quantum size effect, etc., which can not only enhance the light absorption and electron transportation efficiency, but also suitably tailor the light emission wavelength and band gaps efficiently. Thus, the atomic nanostructures exhibit superior electrical and optical performance in optoelectronic nanodevices. To form a semiconductor solid solution nanostructure, the crystallographic parameters, chemical valance and radius of cations or anions of component semiconductors should be generally considered for minimum formation energy and a wide range of composition tuning.[9] The formation of semiconductor solid solution can be regarded as a doping process involving the selective cation and anion substitution. Sometimes, the simultaneous doping/substitution of cation and anion leads to form pseudo-binary solid solution. We can adjust the properties of semiconductor nanostructures through either cation and/or anion doping and the control of their concentration in the whole composition range. That's why the design of material system and the precise control of their reaction process require a well-designed synthetic strategy. Such property customization of semiconductor nanostructures through the alloying of semiconductors with different band gap structures and optoelectronic characteristics provides a powerful platform for the formation of a variety of optoelectronic nanodevices and a fruitful avenue towards the production of clean energy.

In this review, we will firstly give a brief overview on the categories of semiconductor solid solution nanostructures based on their component elements (namely binary, ternary and quaternary) and a more emphasis is given on ternary solid solution nanocrystals for their

abundant material systems, tremendous properties and promising applications. In the second part, various synthetic routines toward the controllable growth of diverse solid solution nanostructures, including nucleation and structure design, morphology and composition variation will be summarized. As a key part, the optical and electrical property tailoring in all kinds of semiconductor solid solution nanostructures through the solubility control in a wide range will be addressed in detail and subsequently, their potential applications in various fields ranging from optoelectronic nanodevices to clean energy harvesting will be discussed. Finally, the challenge and future perspectives in the field of semiconductor solid solution nanostructures and related applications are highlighted.

2. Classification of semiconductor solid solution nanostructures

Semiconductor solid solution is a single phase alloy that is composed of two different semiconductors with the same structure properties and different optoelectronic properties. The formation of semiconductor solid solution should basically follow the following principles:[9] (1) the comprising two semiconductors should have the same crystallographic symmetries and very close lattice constants; the good matching of the two semiconductors in structure and unit cell constants can guarantee their alloying in a wide composition range and to avoid the phase separation due to the large lattice-mismatching strain. Normally, the closer the constants between two semiconductors are, the easier it is to form the solid solution. (2) The two semiconductors should also have very similar chemical properties to promote their combination into a single phase compound. The valence and ion radius of corresponding cations and anions in two semiconductors should have less difference to enable a random substitution. In addition, a well-designed synthesis strategy is also of great importance to obtain the solid solution nanostructures with controllable solubility. The selections of synthetic routine, proper precursors and the precise control of reaction parameters (such as temperature and pressure) are the key factors in optimization of solubility, hence, gives tailor-made band-gap of the semiconductor solid solution nanostructures. In spite of this, when the

over-solubility appears, the semiconductor solid solution separates into two phases in the form of heterostructure, which in turn provides us an approach toward the achievement of semiconductor junctions.[10]

Based on the constituting elements (cation or anion) and their numbers, the semiconductor solid solution nanostructures can be simply classified into (1) binary solid solutions, (2) ternary solid solutions and (3) quaternary solid solutions. Even though the formation principle is the same for all these semiconductor solid solutions as mentioned above, the properties of the three types of semiconductor solid solutions exhibit great disparity, which will be discussed later in detail. After tremendous efforts, a large amount of semiconductor solid solution nanostructures either in binary, ternary or quaternary have been developed in different material systems and **Figure 1** lists the possible elements that comprise these semiconductor solid solutions. Detailed introduction of these representative semiconductor solid solutions is described as follows.

2.1 Binary Semiconductor Solid Solutions

Si_xGe_{1-x} system (Group IV elements), is the only best-known and extensively investigated binary semiconductor solid solution.[11, 12] The identical crystallographic symmetry and close lattice constants of Si (cubic, a=5.431 Å, 1.12 eV) and Ge (cubic, a=5.658 Å, 0.66 eV) theoretically enable the whole composition range flexibility and corresponding band-gap control in the range of 0.66-1.12 eV. Based on the Si_xGe_{1-x} solid solution nanostructures, various optoelectronic and microelectronic devices can be realized through the precise control of their nucleation, composition, dimensional size, optical and electrical property.[13] Takeoka et al.[11] reported $Si_{1-x}Ge_x$ nanocrystals with Ge content in the range of $0 \leq x \leq 0.31$, which is fabricated by the deposition of Si, Ge, and SiO_2 followed with post-annealing treatment at 1100 ºC. Nevertheless, SiH_4 and GeH_4 as Si and Ge precursors in a vapor liquid solid process further broadened the Ge content in the whole composition range of $0 \leq x \leq 1$ and the $Si_{1-x}Ge_x$ nanowires showed excellent crystallinity, adjustable band-gaps and

thermal conductive properties for photodetectors, field effect transistors (FETs) and thermoelectric devices.[14] Further precise control of the SiH_4 and GeH_4 gas precursors during the chemical vapor deposition synthesis can lead to the formation of composition graded $Si_{1-x}Ge_x$ nanowires.[15] The Si and Ge ratio along the axial direction can be selectively and continuously tuned to fully tailor the band-gap and optoelectronic properties in an individual $Si_{1-x}Ge_x$ nanowire. Such single $Si_{1-x}Ge_x$ nanowire with axially graded energy-band opened new frontiers in fabricating high performance photodetectors for selective wavelength detection in a wide range.[13]

2.2 Ternary Semiconductor Solid Solutions

In comparison with binary semiconductor solid solutions, ternary semiconductor solid solution nanostructures exhibit inspiring advantages for their abundant material systems and hence, more versatile properties. Ternary semiconductor solid solutions can be obtained through the combination of two independent binary compounds, which share the same crystal structure, anion or cation. The formation of ternary semiconductor solid solution can also be regarded as an elemental doping process, in which the cation or anion in binary host is substituted by the element in the same group. The large material system of ternary semiconductor solid solutions provides more chances to fully customize the semiconductor properties and more possibilities to realize the potential applications in diverse fields ranging from LED,[16] optoelectronic devices (such as photodetectors and phototransistors),[17, 18] catalysis,[19] lasers,[20] optical waveguide,[21] solar cell,[22] to environmental processing.[23] Based on the elemental constituents, the ternary semiconductor solid solutions can be further classified into (i) II-VI solid solution and (ii) III-V solid solution. The II-VI ternary solid solutions are mainly related to Group IIB cations (Zn, Cd, Hg) and VIA anions (O, S, Se, Te), while the III-V ternary solid solutions are made of the elements from Group IIIA (Al, Ga, In) and VA elements (N, P, As, Sb) in the periodic table, as shown in **Table 1**. In this section, we will mainly introduce the representative $Zn_xCd_{1-x}S$, CdS_xSe_{1-x}, $In_xGa_{1-x}N$ and $Al_xGa_{1-x}N$

material systems as examples of cation and anion doping.

2.2.1 CdS_xSe_{1-x} and $Zn_xCd_{1-x}S$ solid solution nanostructures

CdS_xSe_{1-x} is a key member of the II-VI ternary chalcogenide solid solution, which has attracted widespread attention for its promising application in photo-electronics owing to its excellent properties such as large nonlinear susceptibilities, good photoconduction and fast photo-response time.[24] Because of the smaller lattice mismatch, CdS and CdSe are able to be miscible over a wide range of composition, leading to an efficient band-gap engineering in the range of 1.73 (CdSe)-2.44 eV (CdS). In addition, the smaller enthalpy to form ternary CdS_xSe_{1-x} ($0 \leq x \leq 1$) solid solution also guarantees the wide solubility for effective property tailoring.[25] To synthesize the ternary CdSSe nanostructures, a lot of approaches such as template-assistant (TP) methods,[26] solvothermal,[27] thermal evaporation[28] and chemical vapor deposition (CVD)[29] have been developed. Recently, Zhuang et al.[30] reported the lateral-composition-graded CdSSe semiconductor nanoribbons through an improved source-moving vapor phase route, which allows better morphology control based on an effective composition and band-gap tailoring. Similarly, the incorporation of CdSe into CdS can modulate the band-gap of CdS_xSe_{1-x} alloy in the range of 1.94 - 2.42 eV with x = 0 to 0.62. Later, scroll-like colloidal CdS_xSe_{1-x} nanoplates with a thickness of five monolayers were synthesized by using the mixture of chalcogenide precursors (**Figure 2a-b**) and the S content could be further freely tuned from x = 0 to 0.72, which exhibits corresponding Photoluminescence (PL) emission in the range of 410 - 480 nm (**Figure 2c**).[27]

Apart from CdS_xSe_{1-x} semiconductor solid solution which involves the anion doping, the formation of $Zn_xCd_{1-x}S$ semiconductor solid solution is realized through a cation substitution. The substitution of Cd with Zn in ZnS host enables the emission peak shift from UV (3.7 eV) to visible (2.4 eV) for efficient visible light absorption. The effective band-gap tailoring of $Zn_xCd_{1-x}S$ solid solution nanostructure makes it a competitive candidate for promising applications in photocatalysts for hydrogen production,[19] solid-state lighting[31] and

nanolasers.[32] Zhang et al.[33] reported the first synthesis of ternary $Zn_xCd_{1-x}S$ semiconductor nanorods with hexagonal wurtzite (WZ) structure through superionic conductor (Ag_2S)-mediated growth with $[(C_4H_9)_2NCS_2]_2M$ (M=Zn, Cd) as single-source precursors. In addition, series of hexagonal $Zn_xCd_{1-x}S$ nanoparticles and nanorods with variable compositions ($0 \leq x \leq 1$) were also synthesized in a large scale via thermolysis and solvothermal method for promising photocatalytic water splitting.[19, 34] In contrast to thermal-dynamically stable hexagonal $Zn_xCd_{1-x}S$ phase, metastable cubic zinc-blende (ZB) $Zn_xCd_{1-x}S$ phase with $0 \leq x \leq 1$ have also been reported with high photocatalytic performance.[35] In addition, the substitution of Cd with Zn in CdS host also leads to the coexistence of ZB and WZ phases and their structure transition.[36, 37]

2.2.2 $In_xGa_{1-x}N$ and $Al_xGa_{1-x}N$ solid solution nanostructures

Ternary InGaN and AlGaN of III-V nitride solid solution nanostructures hold great promise in the application of high-efficiency and wavelength tunable LEDs[38, 39] and lasers[40] due to their chemical stability, adjustable band gap and wide luminescence spectrum from UV to IR. Single crystalline $In_xGa_{1-x}N$ and $Al_xGa_{1-x}N$ solid solutions with direct band gaps are also often used as the active layers for generating luminescent light. By controlling the solubility of ternary $In_xGa_{1-x}N$, the key basic three colors of red, green and blue can be obtained. For blue light InGaN LEDs, it shows a commercial efficiency with decent stability, whereas the green and red LEDs with In rich exhibit a fast degraded luminescence efficiency because of the formation of high density dislocations leading to the strong non-radiative recombination.[41] To address this challenge and to develop pure InGaN white LED, Yang et al.[12] synthesized high quality and single crystalline $In_xGa_{1-x}N$ nanowires across the entire composition range from x = 0 to 1 through halide CVD method. PL measurements suggest that a tunable emission wavelength from ~ 390 to 735 nm can be obtained by controlling the In content. The integration of InGaN layer with doped GaN to form n-GaN/InGaN/p-GaN core/shell/shell (CSS) structures by metal organic chemical vapor deposition (MOCVD)

method can further enhance the carriers injection efficiency in a single nanowire photonic device.[42] Concerning deep UV LEDs and lasers, AlGaN solid solution nanostructures exhibit huge potential as the high-efficiency active layer. For instance, semi-polar AlGaN layers epitaxially grown on coalesced GaN nanowire arrays exhibit a quasi 3D film structure and decent crystal quality for achieving high room-temperature luminescence efficiency, superior charge carrier transport properties and excellent electrical and optical performance.[43]

2.3 Quaternary Semiconductor Solid Solutions

Unlike binary and ternary semiconductor solid solutions, quaternary semiconductor solid solution is composed of two binary semiconductors that are made of different cations and anions. The formation of quaternary semiconductor solid solution also involves the simultaneous doping or substitution of cations and anions in host binary semiconductor. The phase separation and local elemental aggregation are rather challenging to avoid along with the homogenous composition control. As a result, the nucleation and crystallization of quaternary semiconductor solid solution are more complicated. Therefore, it is considered essential to confirm the phase purity and composition homogeneity using various characterization techniques. The critical characterizations of the single phase of solid solution nanostructures are feasibly done by X-ray diffraction (XRD) and selective area electron diffraction (SAED) methods. As illustrated in **Figure 3**, which show no peak and diffraction spot splitting; while the elemental distribution inside a solid solution nanowire can be identified from the high-resolution elemental mapping. The quaternary solid solution provides a more useful means to tailor the optoelectronic properties of semiconductor due to the simultaneous doping of cations and anions. Compared with binary and ternary solid solutions, quaternary semiconductor solid solution exhibits some unexpected properties valuable for technological applications in diverse fields. So far, the quaternary semiconductor solid solutions have been reported for groups (II-VI)-(II-VI), (III-V)-(III-V) and (II-VI)-(III-V) material systems which mainly include ZnCdSSe,[44-47] ZnCdSeTe,[48, 49] GaInAsSb,[50] GaN-

ZnO,[51-55] GaP-ZnS,[9, 10, 56, 57] GaP-ZnSe[58] and GaAs-ZnSe.[59]

2.3.1 GaN-ZnO solid solution nanostructures

GaN-ZnO solid solution particles were firstly reported by Maeda et al.[60] in 2005. The nitridation of Ga_2O_3 and ZnO powders directly leads to their alloying to GaN-ZnO solid solution. Interestingly, the GaN-ZnO solid solution showed a fascinating phenomenon of band gap narrowing compared with the wide band gap of initial GaN (3.4 eV) and ZnO (3.37 eV). It was explained that the band-gap reduction is mainly because of the repulsion of Zn *3d* and N *2p* orbitals in the valence band after the formation of quaternary solid solution. Photocatalytic test implies that the GaN-ZnO solid solution is an excellent photocatalyst for overall water splitting for H_2 production under visible light irradiation. Until 2010, one dimensional GaN-ZnO solid solution nanowires were successfully synthesized through the nitridation of homogeneous Ga-Zn-O precursors by Han et al.[61] and the ZnO ratio can be adjusted from 0.088 to 0.482 with the corresponding band gap varying from 2.21 to 2.65 eV. Similar synthetic strategy produced GaN-ZnO solid solution nanowire with a ZnO content of 12% and it exhibits n-type conductivity in FET. Later, Lee et al.[53] further extended the ZnO solubility to the range of 0.3-0.87 and Li et al.[62] optimized the much wider ZnO concentration in the range of 0.18-0.95 in $(GaN)_{1-x}(ZnO)_x$ hollow spheres. These hollow spheres exhibit superior photocatalytic activity for overall water splitting with the highest quantum efficiency of 17.3% under visible light irradiation. In addition, our group also reported the GaN-ZnO solid solution nanorods with controllable crystal facets and tunable ZnO ratios in the range of 0.25-0.95 (**Figure 2h-m**).[55] By carefully controlling the growth temperature and reaction time, the exposed crystal facets of as-prepared $(GaN)_{1-x}(ZnO)_x$ solid solution nanorods could be tuned from non-polar {10-10} to semipolar {10-11} and then finally mixed {10-11} and polar {000-1} planes with ZnO ratio changing from 0.95 to 0.80 and 0.25 (**Figure 2h-m**). The crystal facet tailoring will undoubtedly bring more opportunities to the property adjustment and photocatalytic applications of $(GaN)_{1-x}(ZnO)_x$ solid solution

nanostructures.

2.3.2 GaP-ZnS and GaP-ZnSe solid solution nanostructures

Besides GaN-ZnO system, GaP-ZnS and GaP-ZnSe solid solution nanostructures have also given remarkable attention for their peculiar properties and specific functions. Previous study on GaP-ZnS and GaP-ZnSe films has found that the invasion of small amount of ZnS or ZnSe into GaP host lattice can cause the drastic decrease of electrical conductivity and the band-gap of the solid solution showed a non-linear dependence on their content. The same phenomenon has also been observed in GaP-ZnS and GaP-ZnSe solid solution nanostructures. Our group has reported the synthesis of $(GaP)_{1-x}(ZnS)_x$ with $x<0.07$[9] and $(GaP)_{1-x}(ZnSe)_x$ with $0.182 < x < 0.209$ solid solution nanowires (**Figure 2d-g**) using two-channel CVD method.[58] Later, Park et al.[56] broadened the solubility of $(GaP)_{1-x}(ZnS)_x$ nanowires to the entire composition range of $0 \leq x \leq 1$ using vapor transport method and a continuous phase transition as a dependence of ZnS content has been observed. The $(GaP)_{1-x}(ZnS)_x$ nanowires first exist in the form of ZB ($x < 0.4$), and then the coexistence of ZB and WZ phases ($x = 0.4 - 0.7$), and finally the WZ phase ($x > 0.7$). However, a phase separation from GaP-ZnS system to form GaP/ZnS heterostructure has also been observed with excessive ZnS content in initial precursors.[10] For $(GaP)_{1-x}(ZnSe)_x$ solid solution nanowires, we still observe the band-gap shrinking after the alloying of GaP and ZnSe, similar to the cases in GaP-ZnS and GaN-ZnO solid solution nanostructures.

3. Synthetic strategies of semiconductor solid solutions

The formation of semiconductor solid solutions in principle can be easily understood based on the structure and lattice constant matching of composed semiconductors. However, their nucleation design and composition control in nanoscale are rather difficult and challenging. Especially, the growth dynamics and crystallization process differ hugely when the component elements increase. Therefore, a well-designed reaction routine and a precise control of the growth parameters such as temperature, pressure, precursors, substrate, and

deposition areas are generally required to obtain homogeneous solid solution nanostructures and to avoid any possible phase separation. Sometimes, a modified method or the combination of several reaction technologies are considered for desired solid solution nanostructures having peculiar properties. So far, extensive efforts have been made in developing and exploring suitable and versatile growth methods for the controllable synthesis of various semiconductor solid solution nanostructures.[30, 43, 45] Here, we will summarize the recent progress on the development of growth technology for all these semiconductor solid solution nanostructures.

3.1 Vapor phase transport route

Vapor phase reaction is widely used for the synthesis of various nanostructures, especially for 1D solid solution nanostructures.[29, 63, 64] The characteristics of this approach involve the vapor or gaseous-stated precursors decomposed/evaporated at high temperature and serve as the reactant sources for the subsequent nucleation and crystallization. Based on different reaction mechanism, the vapor phase reaction can be further classified into vapor–liquid–solid (VLS), vapor–solid (VS), vapor–solid–solid (VSS) and others.[51, 62, 65-68] Occasionally, metal catalyst nanoparticles are further utilized to assist the growth and the size control of semiconductor nanostructures. In this way, low dimensional solid solution nanostructures with atomically homogeneous chemical composition and decent crystal quality can be obtained to meet the specific requirement for high performance device application. According to the reaction processes, it can be further divided into two major types: chemical vapor deposition (CVD)[21, 69] including MOCVD,[70, 71] metal organic vapor phase epitaxy (MOVPE),[72, 73] and halide chemical vapor deposition (HCVD) [12, 41, 74] and physical vapor deposition (PVD) including molecular beam epitaxy (MBE),[18, 75, 76] thermal evaporation,[20, 63] magnetron sputtering[77] and chemical beam epitaxy (CBE).[78]

The CVD process provides predominant advantage in the precise control of nucleation size, composition and morphology of the solid solution nanostructures, which is discussed in

details in this section. Typically, the vaporized precursors generated at high temperature are transported via carrier gases to the substrate position and begin to react. In this case, the elements decomposed from the precursors will reorganize and re-bond to the targeted solid solution nanostructures under a careful control of growth temperature, pressure, substrate, gas flowing rate and so on. The facile control of these parameters facilitates the possible growth of a variety of semiconductor solid solution nanostructures. It has been reported that the growth parameters have a significant impact on the growth mechanism, size and morphology, phase and composition of semiconductor solid solution nanostructures.[79, 80] For instance, with regard to the synthesis of ternary InGaAs solid solution nanowires using MOCVD method, precursors such as (trimethylindium (TMI), trimethylgallium (TMG), and arsine (AsH_3)) having higher flow rates generate ternary InGaAs core with In-rich shell, while the precursors with lower flow rates produce binary GaAs core with ternary InGaAs shells.[67] Moreover, InGaN nanowires with variable compositions and band gaps within the different substrate areas were firstly synthesized by Yang's group using HCVD method.[12] Four temperature zones have been created on the substrate using a horizontal single-zone tube furnace and two independently controlled heating elements, as shown in **Figure 4a**. $InCl_3$, $GaCl_3$ and NH_3 were used as the In, Ga and N sources respectively. By changing the growth parameters, single-crystalline $In_xGa_{1-x}N$ nanowires could be grown across the entire compositional range from x = 0 to 1. The CVD method is especially effective to synthesize quaternary solid solution nanostructures made of two different binary compounds. For example, Pan et al. has demonstrated the successful synthesis of a variety of quaternary solid solution nanostructures such as GaInAsSb,[50] GaZnSeAs[59] and ZnCdSSe[46] using this method, in which the binary compound precursors are isolated in two separated transport channels and are transported to the reaction zone at the same time (**Figure 4b**). Using similar method, we have also fabricated GaP-ZnS,[9, 10] GaP-ZnSe[58] and GaN-ZnO solid solution nanowires[55] with variable size and tunable optoelectronic properties.

3.2 Solution-based reactions

Among the solution-based formation processes, hydrothermal (HT) and solvothermal (ST) methods are also popular and have been extensively used in the synthesis of various semiconductor solid solution nanostructures due to their facile operation and simple setup.[27] Typically, the synthesis is conducted in a sealed autoclave at elevated temperature and pressure or in three-neck flask under Ar flux protection.[81, 82] Under such experimental conditions, water and non-aqueous solvents display different properties such as viscosity and dissociation constant which can promote the mass transportation, the control of nucleation and the growth rate as well as morphology during the growth process of nanomaterials.[4] Recently, it has been found that solid-phase superionic conductors such as Ag_2S can catalyze the growth of chalcogenide nanowires/nanorods in solution based on a process known as solution–solid–solid (SSS) growth mechanism.[83, 84] The cations in the superionic conductors serve as a "fluid" with high mobility, which generates vacancies for the dissolution of foreign cations and hetero-growth of the second phase.[85] Hence, the superionic conductor nanoparticles act as the material transfer center during the growth and play a similar role of the "liquid" media in metal-nanoparticle-mediated growth. Base on this mechanism, the Ag_2S-mediated ternary $Zn_xCd_{1-x}S$ nanorods were achieved with the composition tunable over a wide range through changing the ratio of Zn and Cd precursors.[33]

In addition, the solvent of trioctylphosphine oxide (TOPO) is traditionally and widely used as the reaction medium in the synthesis of semiconductor solid solution QDs.[86-88] Recently, it has been substituted by other solvents composed of long-chain alkanes (C16-C20) due to their low cost, low toxicity, more stability in air, and the high boiling points of 300-400 °C. Xing et al.[89] firstly used paraffin liquid and oleic acid as the solvent and ligand instead of expensive and toxic phosphines of TOPO and hexadecylamine (HDA) to prepare high quality ternary CdSeTe solid solution QDs with strong red to NIR emissions. The solution based CdSeTe QDs also demonstrated a PL-QY up to 70% and superior optical

stabilities against temperature change and photobleaching. From above descriptions, it can be concluded that the solution-based method provides more efficient and simple strategy toward the rational synthesis of semiconductor solid solution nanocrystals with tunable morphology, size, composition and band-gaps, which paves a solid way to the future application of semiconductor solid solution nanostructures in photocatalysis and the development of various optoelectronic nanodevices.

3.3 Other synthetic methods

In addition to the above synthesis methods for obtaining semiconductor solid solution nanostructures, the synthetic technologies including sol-gel method,[90] electrospinning (ES) methods,[91] reflux,[82] template-assistant (TP) methods[26] and microwave irradiation[92] have also been reported. However, it should be noted that some modified reaction strategy combining with different processes is often utilized for a controllable synthesis route of semiconductor solid solution nanostructures. A summary of synthesis methods for semiconductor solid solution nanostructures is given in **Table 1**.

4. Optoelectronic Properties

The alloying of different semiconductors with peculiar optoelectronic properties to form single-phase semiconductor solid solution allows for an easily accessible routine toward the realization of desired band structure and optoelectronic properties through effective solubility tuning. In this section, the optical and electrical property tailoring of binary, ternary and quaternary semiconductor solid solution nanostructures will be discussed and summarized in details. Based on these works, it is expected that a general rule in the optical and electrical property engineering of semiconductors can be established for future applications through the design of solid solutions.

4.1. Optical Property tailoring

The band-gap control of semiconductors solid-solution having different semiconductor components with distinct band structures provides a valid and available strategy to modify the

optical properties such as emission wavelength, optical absorption, photoluminescence (PL) intensity and quantum yield (QY). [12, 93, 94] In terms of light emission, semiconductor solid solution nanostructures are capable of realizing the tunable emission wavelength covering UV to IR through the proper design of host/guest semiconductors and the effective solubility designing, which provides abundant building blocks meeting the requirements of diversified electronic nanodevices such as white LEDs, full-spectrum nano-lasers and wavelength-selective photodetectors. To control the type and content of doping element (phase) in the host material can lead to the continuous change of band energy levels and luminescence centers, which in turn enables us to control the emission wavelength of semiconductor solid solutions. For instance, $Al_xGa_{1-x}N$ ternary solid solution nanostructures can be formed with stable and highly efficient light emission ranging from 280 nm to 365 nm, which is promising for deep ultra-violet (DUV) LEDs and lasers.[38, 40] In contrast, $In_xGa_{1-x}N$ nanowires with fully tunable composition ($0 \leqslant x \leqslant 1$) exhibit a strong PL emission from UV (~390 nm) to red light region (~730 nm), as shown in **Figure 5a-c**.[12] Therefore, we can select suitable nitride solid solution nanostructures for specific applications. Similarly, InGaAs and InAsP ternary solid solutions as promising materials for IR detectors have emission wavelengths (at 77 K) of 857-930 and 860-3070 nm, which correspond to near-IR and mid-IR regions, by controlling the compositions, respectively.[80, 95] Additionally, groups IIB-VI and III-V solid solution nanostructures including $ZnS_{1-x}Se_x$, $CdS_{1-x}Se_x$, $Zn_xCd_{1-x}S$, $Zn_xCd_{1-x}Se$, ZnCdSSe, InSbAs, GaPAs also exhibit the wide emission wavelength range in UV-Vis-IR region, as listed in **Table 1**. Generally, the luminescence of semiconductor solid solution nanostructures is mainly produced by the near band edge emission (NBE), which is determined by the band-gap and direct/indirect band structure. In addition, the defects resulting from the alloying of different semiconductors can also create relevant located energy levels for light emission. For example, defect emission in the red region is often observed in Ga-rich InGaN solid solution nanowires, (**Figure 5c**). Nevertheless, the increase of Indium content leads to the fading away

of the defect-related emission in In-rich nanowires. Similar phenomenon is also observed in tetrapod-like ZnSSe nanostructures.[96] To further resolve the defect emission and to make better use of tunable emission wavelength for advanced optoelectronic nanodevices, it is indispensable to improve the crystal quality and decrease the defect density of solid solution nanostructures through a well control of the reaction process.

Except for the emission wavelength, the absorption edge of semiconductors can also be selectively tailored based on the designed nucleation of solid solutions. The increased optical absorption of semiconductors in the visible region can dramatically promote the improvement of solar conversion efficiency (SCE) in the field of solar cells and photocatalysis. As shown in **Figure 5d**, the absorption edge of InGaN ternary solid solution nanowires shifts from 3.3 (~375 nm) to 1.2 eV (~1000 nm) when the In content is controlled from x = 0 to 1, which can be used as a promising photocatalyst for visible-light-driven water splitting.[12, 97] In addition, the absorption edge of ZnCdSSe quaternary solid solution nanowires/nanobelts/nanosheets shifts from 2.88 (~430 nm) to 1.96 eV (~632 nm) with the contents of Cd and S increasing from x=0 to 1.[98] Similarly, the absorption of CdZnTe ternary solid solution quantum dots (QDs) can be modulated in the range of 480-570 nm when the ZnTe ratio increases (**Figure 5e**).[93] Therefore, the band-gap reduction or the improved absorption in visible range of a variety of semiconductors can be realized through the alloying of different semiconductor components and their solubility tailoring in a wide range, as listed in **Table 1**. Additionally, it is also found that the absorption efficiency of semiconductors is strongly affected by the band-gap type of the solid solution nanostructures. For example, the band gap of $In_xGa_{1-x}P$ ternary solid solution nanowires decreases from 2.26 to 1.35 eV when the In content is increased from 0 to 1. Correspondingly, the absorption edge of $In_xGa_{1-x}P$ moves from 400 to 1000 nm.[98] Meanwhile, it was found that an energy band structure transition from direct to indirect appears at x = 0.21 and the InGaP nanowires showed a sharp increase at absorption

edge in direct range (x > 0.21). While, in indirect range (x<0.21), it showed a slow increase at absorption edge due to the direct-indirect band gap transition.

The solubility control of semiconductor solid solution nanostructures makes it possible to freely adjust the optical property (emission wavelength, intensity, etc.) of host semiconductor. However, the emission intensity of semiconductor solid solutions gradually quenches with the increase of solubility to a certain extent. The luminescence depression of semiconductors is also harmful to the corresponding performance of optoelectronic nano-devices like LEDs and lasers.[99] The main reason can be attributed to the increased non-radiation centers induced by the defects and the lattice deformation under high solubility condition. For $Si_{1-x}Ge_x$ QDs with a similar size of ~ 4 nm, the quenching of PL intensity is easily observed with increasing Ge content from 0 to 0.31 due to the rise of Ge P_b defect density.[11] Similarly, the PL intensity of ternary InGaN solid solution also exhibited a decreasing tendency in In-rich region.[12] As a result, it is quite difficult to obtain high efficiency and very bright green/red InGaN LEDs. The quenching of luminescence decreases the QY of semiconductor solid-solution QDs. Therefore, it is essential to prevent the possible luminescence degradation. Previous studies have revealed that prolonging the reaction time could increase the PL-QY of CdZnTe QDs and a maximum QY as high as 65.35% can be obtained with the Zn:Cd=1:1 and the reaction time of 12 h.[94] In addition, the enhancement of QY in solid solution nanostructures can also be realized through modifying some ligands or molecular on the nanostructure surface to decrease surface defect traps. A typical example can be found in CdZnTe QDs through the linking of short RGD peptide ligands on their surface.[93] It has been found that the PL-QY of CdZnTe QDs can reach as high as 60% under optimized reaction conditions.[93]

Compared to semiconductor solid solution nanostructures with homogenous composition, single nanowires/nanoplates with gradient composition show fascinating optical properties including multiple-wavelength light emissions and enhanced optical absorption,[8] which has

attracted extensive attention in the potential applications of white nano-LEDs,[46] photodetectors[13] and lasers.[45] The composition modulation in a single nanowire requires a precise control of the reactants in a well-designed process. Pan et al. demonstrated that the substrate-moving growth approach was quite suitable to realize the gradient composition along the axial direction of ultra-long ZnCdSSe and CdSSe nanowires (**Figure 4c**).[46, 63] Using this method, the composition of CdSSe nanowires can be continuously tuned from x = 0 (CdS) at one end to x = 1 (CdSe) at the other end, and thus a continuous light emission from 507 nm (2.44 eV of CdS, green light) to 710 nm (1.74 eV of CdSe, red light) along the length direction can be obtained.[63] To further integrate red, green and blue emissions in single nanowire for white light devices, Zn element can be introduced to CdSSe system to form ZnCdSSe quaternary nanowires with axial composition-gradient. In this way, the adjustment of red, green and blue emissions for a near-daylight white light emission can be achieved in a single nanowire through the precise composition control along the growth direction.[46] Similar ZnCdSSe nanosheets with full composition-gradient from one side to other side are also promising to achieve red, green and blue lasing light for a monolithic white laser.[45]

4.2. Electrical Properties

The energy band structure is not only related to the optical properties, but also the electrical properties of semiconductors. Therefore, an efficient tailoring of the band-gap structures of semiconductors through the alloying of different semiconductors and their solubility control allows for an accessible approach to adjust the electrical properties. The variation of energy band-gap also affects the effective mass, redox ability of photo-generated electrons/holes, conductivity and so on. The band gap as a dependence of the component in ternary semiconductor solid solutions can be described as follows:

$$E_g^{(A_xB_{1-x}C)} = xE_g^{(AC)} + (1-x)E_g^{(BC)} - bx(1-x)$$

where b is a constant.[12] For quaternary solid-solution ($A_xB_{1-x}C_yD_{1-y}$), the band gap variation follows the function:[100]

$E_g^{(A_xB_{1-x}C_yD_{1-y})} = xyE_g^{(AC)} + (1-x)yE_g^{(BC)} + x(1-y)E_g^{(AD)} + (1-x)(1-y)E_g^{(BD)}$

Apparently, the band gap variation of ternary solid-solution would show a bowing change due to the x^2 part. For example, it has been verified that the band gap of bulk $GaAs_{1-x}P_x$ solid-solution follows the function very well and it exhibits a bowing phenomenon in band gap variation. Theoretical calculation also predicts that a crossover would occur at a given GaP ratio (x=0.5) due to the band gap conversion from direct to indirect. However, for twinned GaAsP ternary nanowires, it shows a linear relationship rather than bowing or crossover variation, which is ascribed to the special twinned super-lattice structures of octahedral slice segments with ZB plane locating between WZ planes.[101] The linear relationship of band gap vs composition is further demonstrated in ternary $WS_{2x}Se_{2-2x}$ nanosheets.[102] As the functions depicted, the band gap of solid-solution has a minimum value in the side of pure binary component. The study of series of solid-solution systems has demonstrated that the band gap could be tailored between the two primitive parts (such as AB and AC for AB_xC_{1-x}). However, an abnormal phenomenon is discovered in quaternary GaP-ZnSe,[58] GaN-ZnO,[55] and GaP-ZnS[57] systems, which exhibited a minimum band gap smaller than that of the pure component semiconductors in the whole composition range. The first principle study on the GaP-ZnS system based on density functional theory (DFT) calculations indicates that the formation of minimum energy band gap is mainly attributed to the shifting up of valence band caused by the repulsion of phosphorus *2p* and zinc *3d* electrons.[57] In addition, the interaction of Ga with S atoms, which decides the conduction position of GaP-ZnS solid solution, induces the downward of conduction position, and finally leading to the band gap shrinking of GaP-ZnS solid solution. The alloying of GaP and ZnS also creates an indirect to direct change of the conductivity during the formation $(GaP)_{1-x}(ZnS)_x$ solid-solution because of the intrinsic conductivity features of GaP and ZnS. Importantly, the change of band structures simultaneously has a significant influence on the redox capability of photo-generated electrons and holes. To achieve maximum photocatalysis efficiency, an optimization of the

band-gap of the solid solution is definitely required through the control of solubility. For instance, the phenol removal efficiency dramatically drops off due to the decrease of oxidation capability of photo-generated holes in $(GaN)_{1-x}(ZnO)_x$ solid solution photocatalysts when the band-gap is adjusted in the range of 2.38-2.76 eV.[23]

The electrical properties of the solid solution nanostructures can also be modified through the customizing of effective mass of electrons and holes, which are also strongly related to the band gap structures and inversely proportional to the mobility of charge carriers.[103, 104] Based on a virtual crystal approximation (VCA) method and the hypothesis of random distribution of atoms in supercell, the calculation of effective mass of electrons (m^*_e) and holes (m^*_h) as well as the mobility of $Si_{1-x}Ge_x$ nanowires finds that the band gap of $Si_{1-x}Ge_x$ nanowires (diameter : 8nm) decreases with the increase of Ge content and a turning point at x = 0.8 is observed.[104] The effective mass of electrons also displays the same tendency as the band gap variation and a turning point for m^*_e arises at x = 0.8. In addition, the hole mobility of solid-solution nanostructures was also reported in CdSeTe nanocrystals.[22] It confirms that the hole mobility in $CdSe_xTe_{1-x}$ solid solution nanocrystals still follows a similar decrease change with the increase of band gap. Additionally, the electrical conductivity of semiconductor solid solutions can be engineered by raising annealing temperature. For example, the hole mobility of CdSe (x=1) enlarges four orders of magnitude from $4.30(\pm1.21)\times10^{-8}$ to $6.88(\pm1.35)\times10^{-4}$ $cm^2V^{-1}s^{-1}$ when the annealing temperature increases from 315°C to 355°C. We can still modify the electrical conductivity and resistivity of semiconductor solid-solutions through the control of component solubility.[105, 106] It has been reported that the electrical resistivity of $(GaP)_{1-x}(ZnSe)_x$ increases greatly with $x<0.4$ and decreases sharply with $x>0.9$.[106] For $(GaP)_{1-x}(ZnS)_x$ solid solution, the electrical resistivity is much larger with $x < 0.1$ and $x > 0.8$ and keeps steadily in the range of $0.1 < x < 0.8$. The $Zn_{1-x}Cd_xS$ nanocrystals also showed a reduction of conductivity as the CdS ratio increases, with an exception at x=0.7.[105] Previous studies have demonstrated that the electrical resistivity and conductivity of semiconductors

are easily affected by the electrons scattering and the trapping in defects. The alloying of two semiconductors with different lattice constants and band structures can easily create numerous structural defects including dislocations and vacancies, resulting in a remarkable decrease of conductivity. For example, the invasion of ZnS with a wider band-gap into GaP host lattice induces the drastic increase of electrical resistivity, leading to the semiconductor to insulator transition of GaP-ZnS nanowires.[9] As a result, the electrical properties including conductivity and resistivity of host semiconductor can be selectively modified through the alloying with suitable guest semiconductor (or elements) and their solubility control.

5. Applications

5.1 Optoelectrionic nanodevices

5.1.1. Light emitting diodes

The candela-class brightness blue LEDs based on ternary solid solution double-heterostructure of InGaN/AlGaN proposed by Shuji Nakamura et al. in 1994[107] have demonstrated a huge breakthrough in the field of blue LEDs and speeded up the development of LEDs toward commercial ultilizations. So far, various LEDs based on thin semiconductor films have played an important and indispensable role in our daily life in terms of lighting and displays. In contrast with film-based LEDs, the nanowire-based LEDs portray a bright future in solid state lighting and displays due to their predominant advantages.[46, 108, 109] On the one hand, the nanowire geometry can relieve the strain stress from the lattice mismatch of substrates and dramatically reduce the threading dislocations density of InGaN and AlGaN solid solution to further decrease the number of non-radiation recombination centers. On the other hand, it is more feasible to intergrate blue, green and red nanowire-based LEDs on one chip and realize truly phosphor-free white LEDs with higher external quantum efficiency (EQE), color gamut and longer time reliability. Lee et al. reported the fabrication of two kinds of single nanowire blue LEDs through the epitaxial growth of c-plane (**Figure 6a$_1$-a$_3$**) and m-plane (**Figure 6a$_4$-a$_6$**) oriented InGaN/GaN multiple quantum wells (MQW) on GaN

nanowires.[110] The comparative electroluminescene (EL) spectrum studies of c-plane and m-plane oriented MQW LEDs with the injection current of 5-50 μA in **Figure 6a$_3$** and **6a$_6$** clearly showed that *m*-plane LEDs had a higher and more stable EL emission intensity than that of *c*-plane LEDs, demonstrating the negative effect of piezoelectric polarization, and the EQE of *c*-plane and *m*-plane oriented MQW LEDs were estimated to be 25 and 35.65% at an injection current of 50 μA, respectively. The luminenscence peaks of 415 and 425 nm demonstrated that the injection current was mainly confined into InGaN active layers for high efficent blue light emission. Correspondingly, the insets of **Figure 6a$_3$ and 6a$_6$** also display the real images of bright blue light emission for the two kinds of LEDs devices. It is expected that the EQE of single nanowire LEDs can be further improved through the optimization of the MQW thichness and numbers.

In addition to single nanowire based LEDs, Mi et al. reported an ultraviolet (UV) LEDs based on nearly dislocation-free AlGaN ternary solid-solution nanowire arrays.[43] As shown in **Figure 6b$_{1\text{-}2}$**, the UV-LEDs are composed of n-type GaN arrays at the bottom and epitaxial p-i-n AlGaN double heterostucture on the top. Mg doped p-$Al_{0.35}Ga_{0.65}N$ and Si doped n-$Al_{0.35}Ga_{0.65}N$ acting as clading layers are designed to improve the radiation reombinaiton efficiency of injection current in the active layer of i-$Al_{0.14}Ga_{0.86}N$. The room-temperature EL spectra (**Figure 6b$_3$)** show a strong emission at 340 nm and a weak emission at 310 nm, which originates from ternary $Al_{0.14}Ga_{0.86}N$ and $Al_{0.35}Ga_{0.65}N$ layers, respectively, and the out power of ~15 W cm^{-2} can be achieved at a current density of 900A cm^{-2}.

Because of the band gap tunability from the near-ultraviolet (NUV) to the near-infrared region (NIR), InGaN ternary solid solution nanostructure showed great potential in the fabrication of white LEDs. In this case, it is easy to achieve white light emission soly by synthesizing gradient InGaN or blue, green and red InGaN ternary solid solutions in one LED device. However, there still remains considerable difficulty and challenge in preparing high quality InGaN alloy with tunable compositions across the entire visible spectrum range. Until

2007, Yang et al. demonstrated a succssful synthsis of highly crystalline $In_xGa_{1-x}N$ nanowires with a full compoition range of x = 0 to 1.[12] Despite of tremendous efforts, phosphor-free InGaN based white LEDs still faces some problems to be addressed in the achievement of commercial EQE of green and red light emissions.[41, 111, 112] On the contrast, semiconductor solid solution QDs with smaller size and decent crystallinity have guradually developed to be an excellent candidate to replace conventional phosphors in the white LED devices due to their outstanding optical properties and higher quantum efficiency (QE).[113-115] For instance, Shen and Tseng et al. developed an one-step synthesis of white-light-emitting $Zn_{0.93}Cd_{0.07}Se$ solid solution QDs, as shown in **Figure 6c$_2$**.[115] The corresponding photoluminenscence (PL) spectra in **Figure 6c$_3$** reveal a strong white-light-emission in the wide range of 376-720 nm and the fluorescence QE of 12%. To prepare the white-light emission device, a single film with optimized concenration of $Zn_{0.93}Cd_{0.07}Se$ QDs blended with polydimethylsiloxane (PDMS) was uniformally coated on glass slide under a 365 nm UV lamp exposure, which displayed bright and stable white-light emission for 10 days shown in **Figure 6c$_1$**. From above results, it can be noticed that semiconductor solid solutions with excellent optical emissions from UV to IR have made significant contributions to high-performance solid-state lighting of LEDs, especially white LED devices. Additionally, the further enhancement of crystal quality, suitable band-gap and precise composition can open up more opportunities to the development of nanosized white LEDs with higher EQE, color rendering index (CRI) and excellent gamut area index (GAI). We believe that the gradient InGaN nanowires and ZnCdSe QDs with superior performance would be promising candidates for white LEDs products in the near futhure.

5.1.2. Nanolasers

In addition to LED applications, nano-lasers based on semiconductor solid solution nanomaterials have also made great impacts in the field of data storage, optical

communications, medical and industrial instrumentation.[30, 32, 116] The nanolasers made of semiconductor solid solution with tunable band-gaps are expected to have a bright future in wavelength-tunable and white nanolasers.[24, 45] Mi et al. has demonstrated an electrically pumped $Al_xGa_{1-x}N$ nanowire laser with 239 and 262.1 nm lasing wavelength in the UV-C band (200-280 nm) and UV-A band (320-340 nm) by controlling Al composition in the solid solution and nanowire resonance cavity structure, which shows great potential to replace the commercial gas He-Cd lasers with obvious disadvantages of large volume and short lifetime.[40]

In terms of visible light tunable nanolasers, ternary solid solutions CdS_xSe_{1-x} and $Zn_xCd_{1-x}S$ have demonstrated the possibility of room-temperature lasing covering the whole UV-Visible spectrum range.[24, 32, 117] Lee et al. reported a controllable synthesis of CdS_xSe_{1-x} and $Zn_xCd_{1-x}S$ nanoribbons with CdS composition ranging from x=0 to 1.[32] Under optical pumping, $Zn_xCd_{1-x}S$ and CdS_xSe_{1-x} nanoribbons can realize continuous light lasing ranging from 340 to 710 nm in the whole composition range. To make better use of wavelength-tunable nanolasers and develop white nanolasers for full-color displaying, it is essential to realize the integration of multi-color/multi-wavelength in a single nanostructure. In this regard, quaternary solid solution of ZnCdSSe nanosheet with three-segment heterostructures emitting red, green and blue light was successfully synthesized through a well-designed growth strategy.[45] When the three segments were illuminated with three beams with adjustable shape and intensity, independent lasing of each RGB color, simultaneous two-color lasing of any two of the three primary colors, and finally simultaneous RGB lasing can be obviously observed from the PL spectra and the side of the quaternary nanosheet. Importantly, the white lasing can be realized in the far field through pumping multi-segment of RGB. Toward the commercialization of tunable nanolasers and white nanolsers, the follow-up research works should be majorly focused on the synthesis of solid solution nanomatreials with high quality and low density defects, as well as device optimization and integration.

5.1.3. Photodetectors

To meet diversified requirements of light detection in different fields like astronomy (UV), automatic control (Visible) and thermal imaging (IR), it is significantly important and meaningful to fabricate photodetectors with various cutoff wavelength responses covering the wide range from UV to IR. Semiconductor solid solution nanomaterials with band gap tunability and high crystallinity show predominant advantages in constructing wavelength-tunable photodetectors with high photoresponsivity and EQE.[18, 80] Indeed, ternary solid solution of ZnS_xSe_{1-x} nanowires with tunable band gaps of 2.7-3.7 eV have been reported for fabricating photodetectors covering the detection wavelength from blue to UV region.[118] Especailly, $ZnS_{0.44}Se_{0.56}$ solid solution shows the highest photoresponsivity of 1.5×10^6 A W^{-1}, a photoconductive gain of 4.5×10^6 and very fast response speed of 520/930 ms. The response speed, which is a crucial parameter in the automatic control filed, can be further improved through the designable formation of heterostructure that takes full advantage of the interface junction to make a significant difference. Yu and Guo et al. have successfully synthesized high-quality CdS/CdS_xSe_{1-x} axial heterostructure nanowires through a CVD method.[119] The photodetector based this heterostructure displayed an excellent performance with response speed of 68/137 μs, which was faster than the 1.6/3.7 ms of pure CdS nanowire. For IR photodetectors, $InAs_xP_{1-x}$ and $In_{1-x}Ga_xAs$ ternary solid solutions have aroused wide interests in the past years.[80, 120] On the basis of VLS growth mechanism and additional ion-exchange process, Pan et al. has fabricated band-selective IR photodetectors using $InAs_xP_{1-x}$ solid solution nanowires with continuous composition control in the range of $0 < x < 1$.[80] These photodetectors exhibited sensitive peak wavelength response in the wide range from 900 to 2900 nm and high EQE of ~10^4-10^5. In addition to $InAs_xP_{1-x}$ photodetectors, ternary $In_{1-x}Ga_xAs$ solid solution nanowires with tunable GaAs concentrations also exhibited superior photodetection to IR light.[120] Although the solid solution nanowire photodetectors exhibit

high device performance and decent band selectivity compared to conventional Si-based photodetectors, tremendous efforts should be futher carried out to realize the device integration and mass production.

5.1.4. Field effect transistors

While considereing FET, semiconductor solid solution nanomaterials are also attractive building blocks due to their excellent electronic properties from band offset to enhanced mobility from 1D/2D confinement effects.[102, 121, 122] For instance, Lieber et al. reported the existence of electron gas in the FET device made of undoped GaN/AlN/$Al_{0.25}Ga_{0.75}N$ nanowire radial-heterostructure.[123] Wang et al. further studied the behavior of electron gas on the GaN/AlGaN core/shell nanowire system with hexagonal and triangular cross sections based on calculation and simulation[121] and it was found that the confinement of electron gas at corners or polar faces was directly dependent on the size and highly anisotropic cross-section of the alloy nanowires.

Despite of tremendous progresses made in the preparation of semiconductor solid solution nanomaterials, the relationship between electrical properties and composition in this solid solution system has not yet been well studied. In this regard, ternary $In_xGa_{1-x}As$ 1D nanowires with entire composition range were synthesized and further fabricated into back-gated FETs.[122] The statistical analysis on the electrical properties reveals that increasing In composition in $In_xGa_{1-x}As$ nanowires leads to a continuous decrease of I_{on}/I_{off} ratio, but the field-effect mobility of electron monotonically increases. To accurately investigate a variety of electrical properties, Datta et al. further demonstrated novel multigate nanowire FETs (NWFETs) integrated with probe electrodes in Hall Bridge geometry based on $In_xGa_{1-x}As$ nanowires.[124] A room-temperature ballistic transport phenomenon was directly observed despite the detrimental impact of side wall scattering in this FET device. Concerning 2D nanosheets of semiconductor solid solution, some unique electronic properties related to the

composition were also discovered. For instance, $WS_{2x}Se_{2-2x}$ nanosheets with complete composition range were synthesized and the back-gated FETs were fabricated, as schematically shown in **Figure 7a**.[102] The output characteristics of a $WS_{2x}Se_{2-2x}$ nanosheet transistor (x=0.813) in **Figure 7b** indicate its good ohmic contact and n-type semiconductor behavior. The identical n-type transfer characteristics under source-drain bias from 0.5-3.0 V are displayed in **Figure 7c**. However, a fascinating transition of transfer behavior from n-type (0.55-1 S atomic ratio) to p-type (0-0.55 S atomic ratio) is discovered with decreasing S composition from 1 to 0 (**Figure 7d**). Meanwhile, the threshold voltage exhibits a continuous decrease tendency (**Figure 7e**), while the field-effect mobility decreases first and then increases when the S atomic ratio increases from 0 to 1 (**Figure 7f**). As a result, it can be concluded that the solid solution nanostructures with tunable composition and electrical properties, either in the form of 1D nanowires or 2D nanosheets, are promising candidates for the design and integration of high performance FETs.

5.2 Energy storage devices

5.2.1. Solar cells

Band gap flexibility and controllability of semiconductor solid solution nanomaterials provide abundant material platforms with suitable band gaps in the fabrication of full-spectrum solar cells.[22, 125-127] Ternary $CdSe_xTe_{1-x}$ colloidal QDs are one of ideal materials for QDs sensitized solar cells (QDSCs).[22, 125-128] Compared to single binary CdSe and CdTe, ternary $CdSe_xTe_{1-x}$ solid solution possesses an enhanced light absorption edge extending to NIR range and higher chemical stability.[126] Based on the type II heterostructure between $CdSe_{0.45}Te_{0.55}$ QDs and TiO_2 electron transfer layer, the excited photoelectrons of $CdSe_{0.45}Te_{0.55}$ light absorbers can efficiently transfer to the conduction band of TiO_2, thus realizing the separation of photogeneraed electrons and holes in solar cell. As a result, the QDSC made of ternary $CdSe_{0.45}Te_{0.55}$ solid solution QDs exhibits a larger current density of 19.35 mA cm^{-2}, an open circuit voltage of 0.571 V and a power conversion efficiency (PCE)

as high as 6.36% under simulated AM 1.5 light illumination (100mW/cm^2), which is much higher than that of single binary CdSe, and CdTe QDs. To further increase the PCE of $CdSe_xTe_{1-x}$ QDSCs, decreasing the trapping states on the surface of QDs is a valid approach to reduce the recombination of electrons and holes. In this regard, a CdSe:Mn layer was introduced on the surface of $CdSe_xTe_{1-x}$ QDs by bath method and the PCE as high as 8.14% can be obtained.[128] In addition, the core/shell structure of $CdSe_xTe_{1-x}$/CdS QDs also showed the possibility to further improve the PCE,[127] and the recorded PCE of 9.48% can be achieved through the further coating of barrier layers of a-TiO_2 and SiO_2 around the sensitized photoanode.

5.3 Photocatalytic applications

In addition to the above-mentioned applications of optoelectronic and energy storage devices, the emerging photocatalysis application of semiconductor solid solution nanomaterials has also aroused global attention in the field of environmental processing and clean energy production. Compared with pure binary semiconductor photocatalyst, solid solution nanostructures can realize the optimization of photocatalysis performance by engineering the band gap on the basis of maintaining adequate redox capability of photogenerated electrons and holes through varying the solubility. In combination with the morphology and size control, it is possible to prepare ideal solid-solution photocatalyst with superior QE toward commercial utilizations. To date, the photocatalytic applications of semiconductor solid solution mainly focus on the field of photodegradation of organic pollutants, photocatalytic and photoelectrochemical (PEC) water splitting.

5.3.1. Photodegradation of organic pollutants

Compared with conventional water processing techniques like physical adsorption, ultra-filtration and electrocatalysis degradation, the degradation of pollutants based on a photocatalytic process possesses superior advantages of low cost and high efficiency in

purifying and decomposing low concentration of organic pollutants (COD < 300). In this case, organic polluants are directly decomposed and oxidized into non-toxic small moleculars and the final production of CO_2 in the presence of semiconductor photocatalysts, light source/sunlight and oxidizing agents of oxygen/air. As shown in Figure 8a_1, the electrons in the valence band can be excited to the conduction band when the photocatalysts are irridated with light possessing higher energy, which simultaneously produces holes with positive charges in the valence band. The generated holes can either directly oxidize organic pollutants or indirectly react with water to produce ·OH radicals for oxidizing contaminents, whereas the corresponding electrons can reduce the absorbed O_2 to form O_2^- and the following ·OH radicals. However, the current UV-sensitive photocatalysts such as TiO_2 and $SrTiO_3$ have a limited utilization of solar energy in spite of their strong redox capability to produce ·OH radicals. On the contrary, semiconductor solid solution provides an accessible approach in tackling this problem through facile band gap engineering.[29, 54, 129] For example, $(GaN)_{1-x}(ZnO)_x$ solid solution photocatalysts discovered by Domen group in 2005 exhibited outstanding visible-light-driven photocatalytic performance.[60] In terms of the photodegradation performance, the removal of four polycyclic aromatic hydrocarbons (PAHs), namely phenanthrene (PHE), anthracene (ANT), acenaphthene (ACE), and benz[a]anthracene (BaA) was investigated in detail using $(GaN)_{1-x}(ZnO)_x$ photocatalyst with Pt modification.[129] It showed excellent activity and stability for the photodegradation of PAHs (PHE>BaA>ANT>ACE) and the loading of Pt nanoparticles leads to an obvious improvement of photocatalytic activity. The mechanism examination evidenced that the degradation of PAHs was induced by the photogenerated holes of $(GaN)_{1-x}(ZnO)_x$ solid solution photocatalyst and active H species derived from the reduction reaction of photogenerated electrons. To further study the solubility (band-gap) dependent photodegradation performance, $(GaN)_{1-x}(ZnO)_x$ solid solution nanocrystals with wide composition range (x=0.25-0.85) and tunable band gap of 2.38-2.76 eV have been

successfully synthesized via sol-gel and nitridation method (**Figure 8a$_1$**).[23] Series of phenol photodegradation experiments revealed that $(GaN)_{0.25}(ZnO)_{0.75}$ has the suitable band gap of 2.76 eV for efficient visible light absorption and powerful photocatalytic capability in removing phenol**.** The loading of 1wt% Ag nanoparticles on $(GaN)_{1-x}(ZnO)_x$ solid solution nanocrystals can further improve the activity of phenol photodegradation with an order of magnitude because of the enhanced photogenerated electrons transfer efficiency at the interfaces (**Figure 8a$_2$**).

In addition to $(GaN)_{1-x}(ZnO)_x$ quaternary solid solution, ternary CdS_xSe_{1-x} nanowires,[29] $Zn_{1-x}Cd_xS$[35] and ZnS_xO_{1-x} nanoparticles[130] were also extensively studied for the removal of organic pollutants like methylene blue (MB) and orange (MO), due to their tunable band gaps and strong visible light absorption in the visible region. The results show that these ternary solid solution photocatalyts possess highly efficient and more stable photodegradation performance under visible light irradiation compared to single binary materials. More importantly, the above works provide more opportunities and insights into fundamental research in developing high efficient visible-light-sensitive photocatalysts for environmental processing. In combination with conventional water processing techniques for high concentration organic pollutants, it will make a big difference and have a bright furture in the filed of water treatments.

5.3.2 Photocatalytic and photoelectrochemical water splitting

Recently, the photocatalytic and photoelectrochemical (PEC) water splitting utilizing solar energy for clean H_2 production have been considered to be an promising strategy to deal with energy crisis. Figure 8b$_1$ shows the schematic diagram of photocatalytic water splitting mechanism. The photoelectrons and photoholes generated inside the semicondctor photocatalysts will be transferred to the surface active sites for water redox reactions. The main challenge of this field roots in the synthesis of highly efficient photocatalysts with broadening visible light absorption and low recombination efficiency for electrons and

holes.[131] In terms of adjustable light absorption, $Zn_{1-x}Cd_xS$ ternary solid solution shows great potentials in photocatalytic water splitting due to its suitable band gap in visible region. In fact, Li and Gong et al. reported the cubic $Zn_{1-x}Cd_xS$ nanocrystals with $0 < x < 1$ and the $Zn_{0.5}Cd_{0.5}S$ sample showed the highest H_2 production rate of 7.42 $mmol \cdot h^{-1} \cdot g^{-1}$ in Na_2S and Na_2SO_3 mixed aqueous solution under visible-light (≥ 400 nm) irradiation.[132] Besides, Mei and Pan et al. fabricated $Zn_{1-x}Cd_xS$ nanocrystals with a nearly full composition ($0.2 < x < 1$) and hexagonal phase and it was found that $Zn_{0.4}Cd_{0.6}S$ showed the highest H_2 production rate of 81 mL h^{-1} g^{-1} in the same condition.[34] To further enhance its photocatalytic performance, an accessible strategy is to decrease the recombination efficiency of photogenerated charges by forming heterojunction and cocatalytst decoration.[19, 36, 133] In this regard, Liu and Guo et al. prepared a new kind of nanotwinned $Zn_{0.5}Cd_{0.5}S$ photocatalyst with NiS_x cocatalyst decoration.[133] The photocatalytic experimental results demonstrated that a superior H_2 production rate of 44.6 mmol h^{-1} g^{-1} and an internal quantum efficiency (IQE) approaching 100% could be achieved at a wavelength of 425 nm light irradiation in the presence of Na_2S and Na_2SO_3 as hole scavenges.

In spite of a superior IQE for photocatalytic H_2 production, the demand of Na_2S and Na_2SO_3 hole scavenges and the existence of photocorrosion for $Zn_{1-x}Cd_xS$ solid solution greatly limit its commercial use. The finding of $(GaN)_{1-x}(ZnO)_x$ quaternary solid solution has been considered as a breakthrough for visible-light-driven overall water splitting for H_2 and O_2 production.[60, 134] After tremendous efforts in the improvement of the light absorption and cocatalyst decoration, Maeda and Domen et al realized a recorded H_2 and O_2 production rate of 3.09 and 1.53 mmol h^{-1} g^{-1} and the IQE of 5.9% in $(GaN)_{0.82}(ZnO)_{0.18}$ solid solution bulk-powder photocatalysts decorated with $Rh_{2-y}Cr_yO_3$ cocatalyst (2.5wt% Rh, 2wt% Cr) and post-calcined at 823 K.[135] Based on this work, Li and Zhu et al. further increased the IQE from 5.9% to 17.3% through delaying the charge recombination and increasing active sites via the size reduction of $(GaN)_{1-x}(ZnO)_x$ photocatalyst.[62] **Figure 8b$_2$** shows the typical overall water

splitting under visible light ($\lambda \geq 400$ nm) for $(GaN)_{0.82}(ZnO)_{0.18}$ nanostructures. The long time test of lasting half a year revealed a only 50% loss of the initial activity, and the regeneration activity could be up to 80% of the initial activity again after reloading $Rh_{2-y}Cr_yO_3$ cocatalyst, which further indicates the excellent stability and durability of $(GaN)_{1-x}(ZnO)_x$.[136] In addition to quaternary $(GaN)_{1-x}(ZnO)_x$, ternary InGaN nanowire with broadening visible light absorption and excellent chemical inerteness was also an interesting material for overall water splititing, which also shows an excellent photocatalytic activity. [97]

Comaperd with photocatlytic water splitting, PEC is another efficient approach to realize water splitting for H_2 production and it has been considered to be possible for commercial utilization at present if combining with photovoltaics. Different from the mechanism of photocatalytic water splitiing, the excited electrons in the semiconductor photoanode are directly transferred to cathode for water reduction, whereas the left holes move to the surface active sites of photocatalysts to oxidize water for O_2 production (**Figure 8c$_1$**). Simultaneously, the external voltage of PEC can compensate the inappropriate conduction/valence band positions and insufficient overpotentials of photocatalyst in photocatalytic water splitting, dramatically improving the separation efficiency of photogenerated charges and finally achieving superior IQE and SCE.[131] In this filed, Sung and Lee et al. fabricated full composition CdS_xSe_{1-x} layer with sensitive TiO_2 nanowire arrays as efficient photoanodes. The formation of type II heterostructure between CdS_xSe_{1-x} and TiO_2 facilitated sufficient absorption of solar light and efficient separation of electrons and holes. The $CdS_{0.2}Se_{0.8}/TiO_2$ sample showed the highest photocurrent density of 6.8 $mAcm^{-2}$ and H_2 generation rate of 600 $\mu mol\ cm^{-2}\ h^{-1}$ (**Figure 8c$_2$**) in 1M Na_2S solution under visible light irradiation (100 $mW\ cm^{-2}$).[137] On the basis of the same considerations, Yang group proposed a modified core/shell structure made of Si/InGaN hierarchical nanowire arrays as photoanode for enhanced PEC water splitting.[74]

6. Conclusion

In summary, semiconductor solid solution has attracted considerable attention and achieved great progress in the aspects of material preparation, property tailoring and applications over the past decades. After tremendous efforts, the family of semiconductor solid solution has been broadened from simple binary-system (SiGe) to abundant ternary-system (ZnCdS, CdSSe, InGaN, GaPAs, etc.) and then complicated quaternary-system (ZnCdSSe, GaN-ZnO, GaP-ZnS, GaAs-ZnSe, etc.). More importantly, semiconductor solid solution nanostructures including nanowires, nanosheets, QDs, etc. have emerged to be the research focus compared to their traditional films and bulk powders. The formation principle based on structure symmetry and crystal lattice matching is concluded for solid solution nanostructures and series of synthetic technologies for obtaining the solid solution nanostructures with controllable solubility have been developed. Up till now, various semiconductor solid solution nanostructures with different morphology and wide solubilities have been obtained as shown in **Table 1**, which can realize the flexible and efficient tailoring of band gaps, optical and electrical properties in a large range. In addition, some peculiar phenomenon like band-gap shrinking and drastic change of electrical properties has been observed in the quaternary solid solution nanostructures. Based on the excellent and tremendous properties, semiconductor solid solution nanostructures have been widely used for the fabrication of high-performance and sensitive optoelectronic nanodevices, the harvesting of clean energy, and the photodegradation of organic pollutants, which exhibits an enhanced performance compared to semiconductor components.

Despite of the significant progress in the design and effective property tailoring of semiconductor solid solution nanostructures, there are still some challenges in achieving the alloyed semiconductors with decent crystal quality, accurate composition and fully-tailoring band-gaps in most material system. In most cases, the band-gap engineering and related property tuning can only be realized in a given composition region far beyond our expectation for the device integration. Even though the continuous band-gap tailoring has been observed

in some semiconductor solid solutions, the structure defect generated from the lattice constant difference will degrade the corresponding optoelectronic properties to some extent. Therefore, some state-of-the-art technology for synthesizing high-quality semiconductor solid solution nanostructures should be developed to solve these issues for further enhancing the properties. In addition, the fundamental understanding of the mechanism for any abnormal property in semiconductor solid solution nanostructures should be further comprehended based on more pervasive experimental evidences in atomic scale. For instance, the smaller band-gap and the drastic increase of resistance in quaternary semiconductor solid solution nanostructures need further investigation in theory and experiment to disclose the exact mechanism. The exact substitutions of cation and anion in quaternary semiconductor solid solution and their effect on the band structures should be clarified. In addition, the contradiction of structural matching and valance state matching in quaternary solid solutions made of group IIIA-VA and IIB-VIA elements still requires more deep and systematic theoretical explorations to disclose the formation mechanism of this complicated material system. In other words, the electron charges inside the quaternary solid solution can not maintain stable when the solid solution is structurally balanced with stoichiometic ratios of cations and anions. On the contrary, the equilibrium of electron charges in the quaternary solid solution will lead to the instability of structure, which will in turn produce large amount of structural defects such as vacancies.

The alloying of different semiconductors into a solid solution has been demonstrated as a powerful way to tailor the band gap and related optoelectronic properties of semiconductors, and various applications have been realized. It is anticipated that the properties of semiconductor solid solution nanostructures can be further enhanced to meet the requirements of diverse applications if the above-mentioned challenges can be effectively addressed. For example, for the epitaxial growth of solid solution nanowires, it is essential to choose suitable substrates with smaller lattice and thermal expansion mismatching coefficient to decrease the density of misfit dislocations. With regard to solid solution nanostructures containing volatile

elements like Zn, As, etc., the concentration of cation or anion vacancies generally appear to be much higher than that in ordinary solid solutions. As a result, it is important to optimize the growth temperature and carry out subsequent annealing process to decrease the vacancy density which influences the optical and electrical properties. Additionally, it is also expected to develop some innovative approach to improve the quality of semiconductor solid solution nanostructures with a low density of defects and wide solubility range. Semiconductor solid solutions with excellent optical, electrical and band gap tunable properties have made great contributions in the development of versatile applications. Among them, LEDs based on ternary InGaN and AlGaN single crystal film have changed our life style. Based on the improved synthesis technology and properties, it is believed that semiconductor solid solution nanostructrured LEDs, lasers and photodetectors will play an important role in the field of displaying, medical micro-instruments, and robots in the near future. In the other field of solar cells and photocatalysis, semiconductor solid solution nanostructures can also provide a good platform for the fundamental research. Finally, it is expected that more semiconductor solid solution systems with accurate property tuning will be created for the promising and advanced applications in a variety of fields.

Acknowledgements

This work was partially supported by the Knowledge Innovation Program of Institute of Metal Research, Chinese Academy of Sciences with grants No. Y2NCA111A1 and Y3NCA111A1, the Youth Innovation Promotion Association, Chinese Academy of Sciences (Grant No.Y4NC711171) and the Basic Science Innovation Program of Shenyang National Laboratory for Materials Science (Grant No. Y4NC6R1161).

Received: ((will be filled in by the editorial staff))

Revised: ((will be filled in by the editorial staff))

Published online: ((will be filled in by the editorial staff))

Table 1. Summary of all the solid solution nanostructures.

Classification	Materials	Methods	Composition range	Emission peaks	Band gaps	Ref.
Binary solid solution	$Si_{1-x}Ge_x$	CVD, MBE, TP	$0 \le x \le 1$	820~962 nm	1.29~1.5 eV	[13-15, 138, 139]
Ternary solid solution	$Al_xGa_{1-x}N$	MOCVD, CVD, MBE	$0 \le x \le 1$	210-365 nm	3.7～6.2 eV	[39, 40, 43, 140]
	CdS_xSe_{1-x}	CVD, TP, ED	$0 \le x \le 1$	507~710 nm	1.74~2.44 eV	[21, 26, 27, 29, 30]
	$In_xGa_{1-x}N$	MBE, MOCVD, HCVD, MOVPE	$0 \le x \le 1$	380-720 nm	1.12~3.43 eV	[12, 66, 74, 141, 142]
	$In_xGa_{1-x}As$	MOCVD, CVD, MBE	$0.01 \le x \le 0.85$	857~930 nm	0.36~1.4 eV	[120, 124, 143]
	$In_xGa_{1-x}P$	MOVPE, MBE, ST	$0 \le x \le 1$	580~950 nm	1.35~2.26 eV	[98, 144, 145]
	$Zn_xCd_{1-x}Te$	ST, CVD, HT	$0 \le x \le 1$	490~660 nm	1.88~2.53 eV	[93, 94, 146]
	$Zn_{1-x}Cd_xS$	HT, CVD, ST	$0 \le x \le 1$	428~590 nm	2.14~3.4 eV	[19, 32-36]
	$Zn_{1-x}Cd_xSe$	ST, CVD, HT	$0 \le x \le 1$	425~540 nm	1.74~2.67 eV	[115, 147, 148]
	$ZnSe_xTe_{1-x}$	MBE, ST, HT	$0 \le x \le 1$	430~467 nm	2.09~2.87 eV	[149-151]
	$ZnS_{1-x}Se_x$	CVD, MOCVD, ST, ES	$0 \le x \le 1$	325~475 nm	2.70~3.5 eV	[91, 96, 152, 153]
	$CdSe_xTe_{1-x}$	HT, ST	$0 \le x \le 1$	600~830 nm	1.48~1.73 eV	[22, 89, 154, 155]
	$InP_{1-x}Sb_x$	MOVPE	$0 \le x \le 0.27$			[65, 156]
	$InAs_{1-x}Sb_x$	MBE, MOVPE, MOCVD, ST,	$0.04 \le x \le 0.875$	770~870 nm	0.18~0.38 eV	[18, 68, 71, 75, 78]
	$GaAs_{1-x}Sb_x$	MBE, MOVPE, CVD	$0 \le x \le 0.93$	844~1760 nm	0.71~1.47 eV	[157-159]
	$Al_xGa_{1-x}P$	MOVPE	$0.05 \le x \le 0.28$	580~950 nm	1.35~2.26 eV	[73]
	$InP_{1-x}As_x$	CVD, MOVPE, MBE	$0 \le x \le 1$	860~3070 nm	0.35~1.42 eV	[76, 80, 160, 161]
	ZnO_xS_{1-x}	HT	$0 \le x \le 1$	380nm,490nm	2.7 eV	[130, 162, 163]
	$Cd_{1-x}Hg_xTe$	reflux, HT,	$0.15 \le x \le 0.85$	712~852 nm	1.45~1.74 eV	[82, 164, 165]
	$Ga_xIn_{1-x}Sb$	MOVPE	$0 \le x \le 1$			[166]
	$GaAs_{1-x}P_x$	MBE, MOVPE, CVD	$0 \le x \le 1$	653~873 nm	1.35~2.23 eV	[79, 167, 168]
Quaternary solid-solution	$(GaN)_{1-x}(ZnO)_x$	CVD, TP, ES, ST	$0 \le x \le 1$	410~505 nm	2.2~2.7 eV	[23, 51-55, 61, 62]
	GaZnSeAs	CVD	-	470~832 nm	1.49~2.64 eV	[59]
	ZnCdSSe	ST, PLD, CVD	$0 \le x \le 1$	350~710 nm	1.75~3.55 eV	[44-47, 169]
	$(GaP)_{1-x}(ZnS)_x$	CVD	$0 \le x \le 1$	345~729 nm	2.4~3.6 eV	[9, 10, 56, 57]
	$(GaP)_{1-x}(ZnSe)_x$	CVD	$0.1 \le x \le 0.9$	550~650 nm	1.95~2.2 eV	[58]
	$Zn_{1-x}Cd_xSe_{1-y}Te_y$	MBE	x=0.13, y=0.02	532 nm		[48, 49]
	$Ga_{1-x}In_xAs_{1-y}Sb_y$	CVD	x=0.35, y=0.33			[50]

Figures

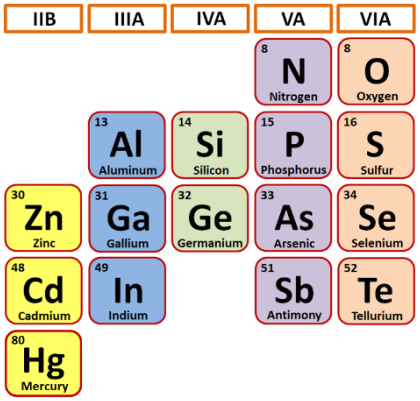

Figure 1. The elements in the periodic table to form possible semiconductor solid solution in this review.

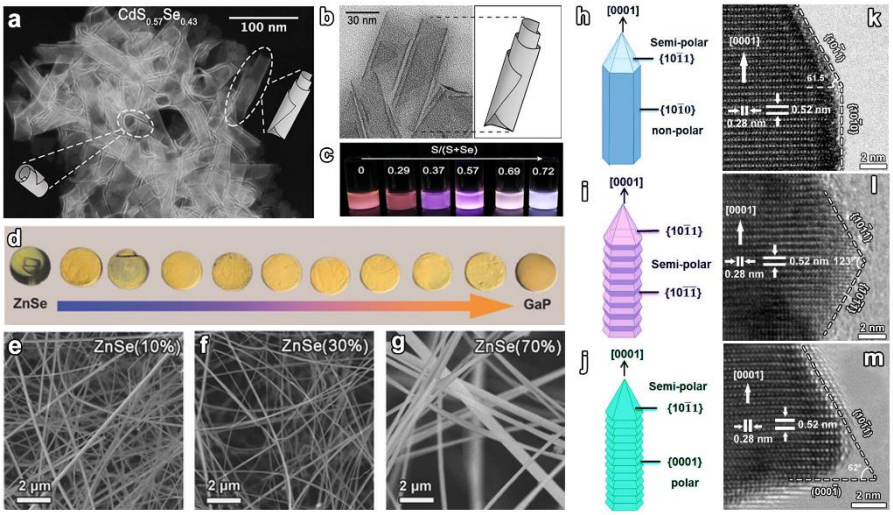

Figure 2. (a) STEM-HAADF and (b) TEM and schematic illustration images of $CdS_{1-x}Se_x$ nanoplates; (c) Corresponding photograph of samples under UV light. Reproduced with permission.[27] copy right 2017, ACS; (d) Real photograph and (e-g) typical SEM images of GaP-ZnSe solid-solution nanowires with different ZnSe ratios. Reproduced with permission.[58] copy right 2015, WILEY. (h-j) Schematic illustration and (k-m) typical HRTEM images of three WZ GaN-ZnO nanorods with different percentages of {10-10}, {10-11} and {000-1} facets. Reproduced with permission.[55] copy right 2016, RSC.

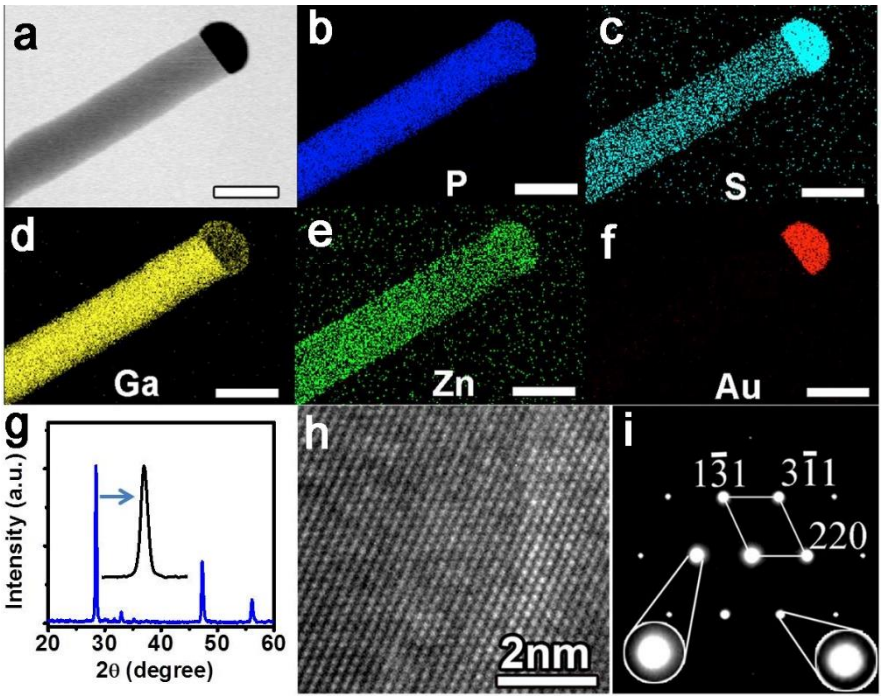

Figure 3. (a) STEM image of an Au-catalyzed GaP-ZnS solid solution nanowire; (b-f) spatially resolved elemental mappings of P, S, Ga, Zn and Au, respectively; (g-i) XRD, HRTEM and SAED pattern of GaP-ZnS solid solution nanowire. Reproduced with permission.[9] copy right 2013, ACS.

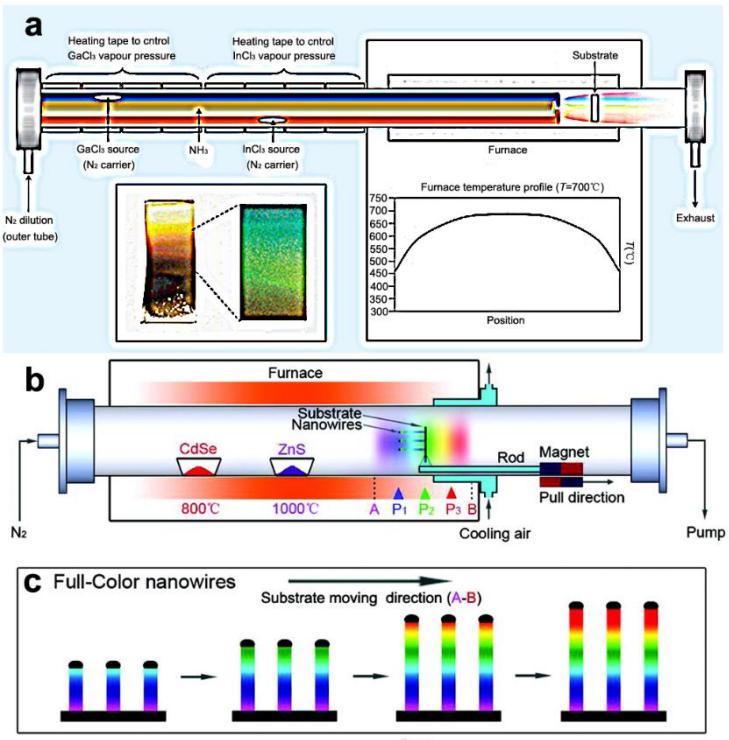

Figure 4. (a) Experimental CVD set-up consisting of three inner quartz tubes which supply the reactive gases, $InCl_3$, $GaCl_3$ (N_2 carrier) and NH_3, and two independently controlled heating tapes which tunes the vapour pressure of the $InCl_3$ and $GaCl_3$ precursors, respectivly. Inset: photograph of an sample on quartz and a PL image from a section of substrate (right). Reproduced with permission.[12] copy right 2007, Nature Publishing Group. (b) Experimental CVD setup and (c) the growth processes for composition and band gap graded ZnCdSSe nanowires, respectively. Reproduced with permission.[46] copy right 2011, ACS.

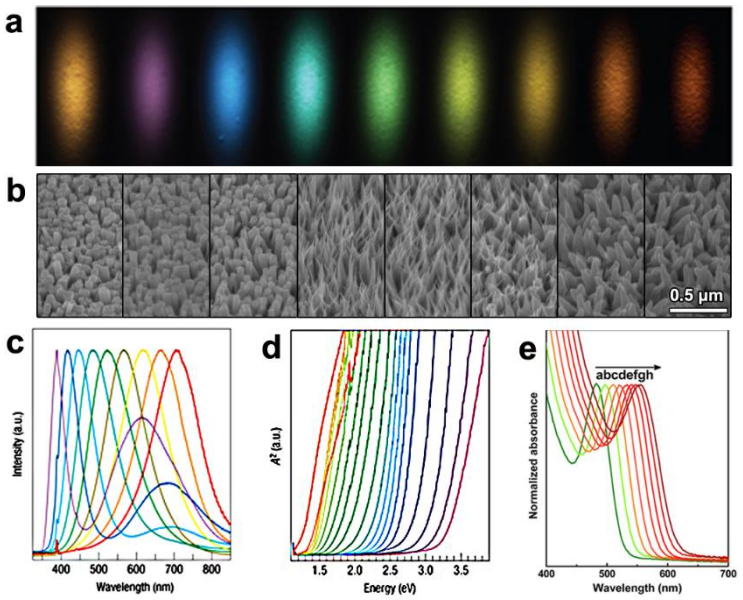

Figure 5. (a) Color CCD image and (b) SEM images of $In_xGa_{1-x}N$ nanowires with x = 2.8%, 10.5%, 25.0%, 33.5%, 36.7%, 53.3%, 64.4%, and 72.4%, respectively (from left to right). (c) Visible PL emissions (x=0-0.6) and (d) optical absorption spectra (x=0-1.0) of the $In_xGa_{1-x}N$ nanowire arrays taken at intervals across the substrates. Reproduced with permission.[12] Copyright 2007, Nature Publishing Group. (e) Temporal evolution of the absorption spectra of (CRGDS+Cys)-capped CdZnTe QDs, respectively. Note that the ratio of CRGDS and Cys was 1:1. Reproduced with permission.[93] Copyright 2012, ACS.

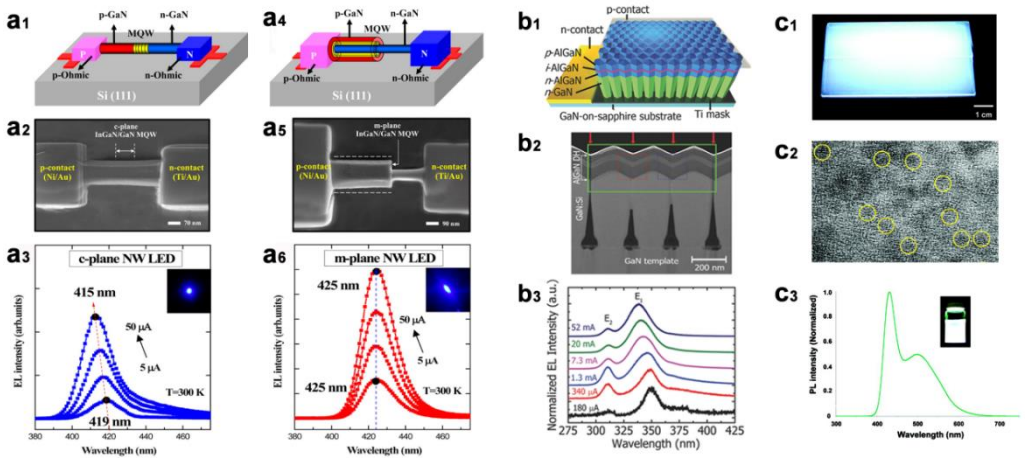

Figure 6. Schematic illustration and top-view FE-SEM images showing the parallel assembly fabrication of ($a_{1\text{-}2}$) c-plane oriented LED and ($a_{4\text{-}5}$) m-plane oriented LED with p-GaN/InGaN/GaN/n-GaN NW structure; (a_3, a_6) Corresponding EL emission spectra. Reproduced with permission.[110] Copy right 2014, ACS. (b_1) Schematic illustration, (b_2) STEM-HAADF image and (b_3) EL spectra of semipolar AlGaN LED device; Reproduced with permission.[43] Copy right 2016, WILEY. (c_1) Thin coating of the $Zn_{0.93}Cd_{0.07}Se$ QDs on a glass slide illuminated by a commercial UV lamp; (c_2) High resolution transmission electron microscopy (HRTEM) image of the $Zn_{0.93}Cd_{0.07}Se$ QDs. (c_3) Corresponding PL spectrum; Reproduced with permission.[115] Copy right 2009, ACS.

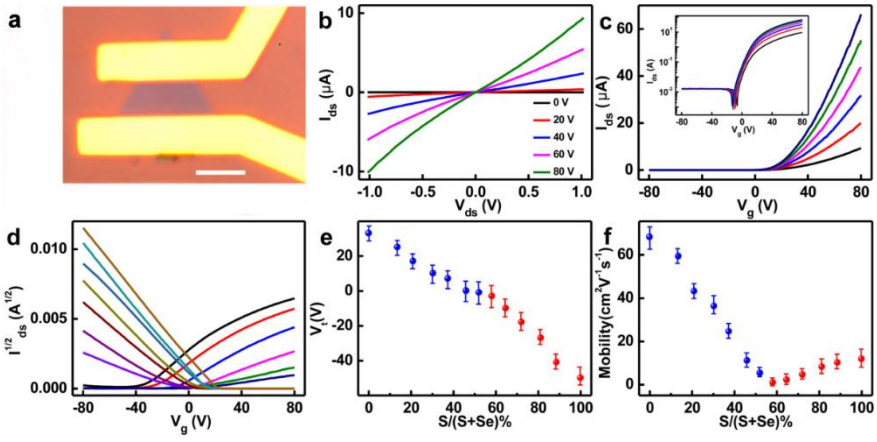

Figure 7. (a) Optical microscopy image and (b) output characteristics of a typical back-gated FET made of a $WS_{2x}Se_{2-2x}$ nanosheet (x=0.813; scale bar = 5 μm). (c) Corresponding transfer characteristics; inset, log plot of I_{ds}-V_g curve. (d) Transfer characteristics, (e) threshold voltage (V_t) and (f) field effect mobility of $WS_{2x}Se_{2-2x}$ nanosheet transistors with different S

atomic ratios from nearly pure WSe_2 (brown curve) to nearly pure WS_2 (black curve). Reproduced with permission.[102] Copy right 2016, ACS.

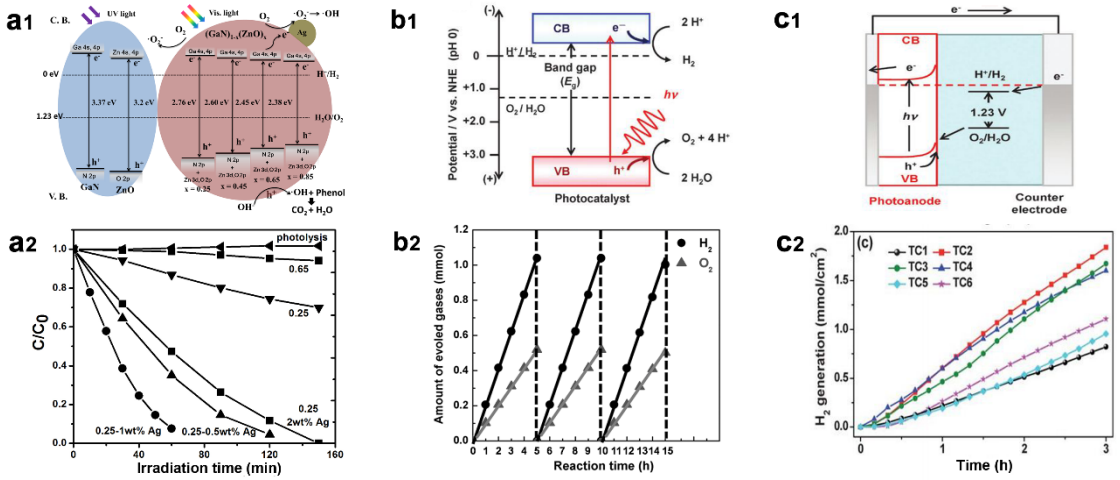

Figure 8. (a_1) Schematic illustration and (a_2) real phenol phototdegradation performance over $(GaN)_{1-x}(ZnO)_x$/Ag composites under visible light irradiation. ($\lambda \geq 400$ nm; 100 mW cm^{-2}; phenol concentration: 10 mg mL^{-1}) Reproduced with permission.[23] Copy right 2017, RSC. Schematic illustrations of (b_1) photocatalytic and (c_1) PEC water splitting. Reproduced with permission.[131] Copy right 2014, RSC. (b_2)Typical overall water splitting under visible light ($\lambda \geq 400$ nm) on the $(GaN)_{0.82}(ZnO)_{0.18}$ nanostructures. Reproduced with permission.[62] Copy right 2014, WILEY. (c_2)Time-dependent H_2 evolution at a potential of 0.5 V using NC samples (TC1–TC6) as the photoanodes. Reproduced with permission.[137] Copy right 2014, RSC.

References

1. K. Sivula; R. van de Krol, *Nat. Rev. Mater.* **2016,** *1*, 15010.
2. T. J. Kempa; R. W. Day; S. K. Kim; H. G. Park; C. M. Lieber, *Energ. Environ. Sci.* **2013,** *6* (3), 719.
3. A. I. Hochbaum; P. Yang, *Chem.Rev.* **2009,** *110* (1), 527-546.
4. N. P. Dasgupta; J. Sun; C. Liu; S. Brittman; S. C. Andrews; J. Lim; H. Gao; R. Yan; P. Yang, *Adv. Mater.* **2014,** *26* (14), 2137-2184.
5. A. H. Chin; T. S. Ahn; H. Li; S. Vaddiraju; C. J. Bardeen; C. Z. Ning; M. K. Sunkara, *Nano Lett.* **2007,** *7* (3), 626-631.
6. H. Sonomura; T. Uragaki; T. Miyauchi, *Jpn. J. Appl. Phys.* **1973,** *12* (7), 968-973.
7. L. W. Yin; S. T. Lee, *Nano Lett.* **2009,** *9* (3), 957-963.
8. X. Zhuang; C. Z. Ning; A. Pan, *Adv. Mater.* **2012,** *24* (1), 13-33.

9. B. Liu; Y. Bando; L. Liu; J. Zhao; M. Masanori; X. Jiang; D. Golberg, *Nano Lett.* **2013,** *13* (1), 85-90.
10. B. Liu; Y. Bando; B. Dierre; T. Sekiguchi; D. Golberg; X. Jiang, *ACS Appl. Mater. Interfaces* **2013,** *5* (18), 9199-9204.
11. S. Takeoka; K. Toshikiyo; M. Fujii; S. Hayashi; K. Yamamoto, *Phys. Rev. B* **2000,** *61* (23), 15988-15992.
12. T. Kuykendall; P. Ulrich; S. Aloni; P. Yang, *Nat. Mater.* **2007,** *6* (12), 951-956.
13. C. J. Kim; H. S. Lee; Y. J. Cho; J. E. Yang; R. R. Lee; J. K. Lee; M. H. Jo, *Adv. Mater.* **2011,** *23* (8), 1025-1029.
14. J. E. Yang; C. B. Jin; C. J. Kim; M. H. Jo, *Nano Lett.* **2006,** *6* (12), 2679-2684.
15. J. E. Yang; W. H. Park; C. J. Kim; Z. H. Kim; M. H. Jo, *Appl. Phys. Lett.* **2008,** *92* (26), 263111.
16. X. B. Tang; G. M. Li; S. M. Zhou, *Nano Lett.* **2013,** *13* (11), 5046-5050.
17. J. Svensson; N. Anttu; N. Vainorius; B. M. Borg; L. E. Wernersson, *Nano Lett.* **2013,** *13* (4), 1380-1385.
18. M. D. Thompson; A. Alhodaib; A. P. Craig; A. Robson; A. Aziz; A. Krier; J. Svensson; L. E. Wernersson; A. M. Sanchez; A. R. J. Marshall, *Nano Lett.* **2016,** *16* (1), 182-187.
19. Z. Mei; B. Zhang; J. Zheng; S. Yuan; Z. Zhuo; X. Meng; Z. Chen; K. Amine; W. Yang; L. W. Wang; W. Wang; S. Wang; Q. Gong; J. Li; F. S. Liu; F. Pan, *Nano Energy* **2016,** *26*, 405-416.
20. Z. C. Liu; L. J. Yin; H. Ning; Z. Y. Yang; L. M. Tong; C. Z. Ning, *Nano Lett.* **2013,** *13* (10), 4945-4950.
21. F. X. Gu; H. K. Yu; W. Fang; L. M. Tong, *Appl. Phys. Lett.* **2011,** *99* (18).
22. Q. Zeng; Z. Chen; Y. Zhao; X. Du; F. Liu; G. Jin; F. Dong; H. Zhang; B. Yang, *ACS Appl. Mater. Interfaces* **2015,** *7* (41), 23223-23230.
23. A. Wu; J. Li; B. Liu; W. Yang; Y. Jiang; L. Liu; X. Zhang; C. Xiong; X. Jiang, *Dalton Trans.* **2017,** *46* (8), 2643-2652.
24. A. Pan; W. Zhou; E. S. Leong; R. Liu; A. H. Chin; B. Zou; C. Z. Ning, *Nano Lett.* **2009,** *9* (2), 784-788.
25. M. A. Hossain; J. R. Jennings; N. Mathews; Q. Wang, *Phys. Chem. Chem. Phys.* **2012,** *14* (19), 7154-7161.
26. Y. Liang; L. Zhai; X. Zhao; D. Xu, *J. Phys. Chem. B.* **2005,** *109* (15), 7120-7123.
27. N. N. Schlenskaya; Y. Yao; T. Mano; T. Kuroda; A. V. Garshev; V. F. Kozlovskii; A. M. Gaskov; R. B. Vasiliev; K. Sakoda, *Chem. Mater.* **2017,** *29* (2), 579-586.
28. P. Guo; X. Zhuang; J. Xu; Q. Zhang; W. Hu; X. Zhu; X. Wang; Q. Wan; P. He; H. Zhou; A. Pan, *Nano Lett.* **2013,** *13* (3), 1251-1256.
29. J. Pan; M. I. Utama; Q. Zhang; X. Liu; B. Peng; L. M. Wong; T. C. Sum; S. Wang; Q. Xiong, *Adv. Mater.* **2012,** *24* (30), 4151-4156.
30. X. Zhuang; P. Guo; Q. Zhang; H. Liu; D. Li; W. Hu; X. Zhu; H. Zhou; A. Pan, *Nano Res.* **2016,** *9* (4), 933-941.
31. T. E. Rosson; S. M. Claiborne; J. R. McBride; B. S. Stratton; S. J. Rosenthal, *J. Am. Chem. Soc.* **2012,** *134* (19), 8006-8009.
32. J. A. Zapien; Y. K. Liu; Y. Y. Shan; H. Tang; C. S. Lee; S. T. Lee, *Appl. Phys. Lett.* **2007,** *90* (21), 213114.
33. Y. Zhang; J. Cai; T. Ji; Q. Wu; Y. Xu; X. Wang; T. Sun; L. Yang; Z. Hu, *Nano Res.* **2015,** *8* (2), 584-591.
34. Z. Mei; M. Zhang; J. Schneider; W. Wang; N. Zhang; Y. Su; B. Chen; S. Wang; A. L. Rogach; F. Pan, *Catal. Sci. Technol.* **2017,** *7* (4), 982-987.
35. D. H. Wang; L. Wang; A. W. Xu, *Nanoscale* **2012,** *4* (6), 2046-2053.

36. Y. Y. Hsu; N. T. Suen; C. C. Chang; S. F. Hung; C. L. Chen; T. S. Chan; C. L. Dong; C. C. Chan; S. Y. Chen; H. M. Chen, *ACS Appl. Mater. Interfaces* **2015,** *7* (40), 22558-22569.
37. W. Wang; I. Germanenko; M. S. El-Shall, *Chem. Mater.* **2002,** *14* (7), 3028-3033.
38. X. Tang; G. Li; S. Zhou, *Nano Lett.* **2013,** *13* (11), 5046-5050.
39. Y. Taniyasu; M. Kasu; T. Makimoto, *Nature* **2006,** *441* (7091), 325-328.
40. K. H. Li; X. Liu; Q. Wang; S. Zhao; Z. Mi, *Nat. Nanotech.* **2015,** *10* (2), 140-144.
41. C. Hahn; Z. Zhang; A. Fu; C. H. Wu; Y. J. Hwang; D. J. Gargas; P. Yang, *ACS Nano* **2011,** *5* (5), 3970-3976.
42. F. Qian; Y. Li; S. Gradečak; D. Wang; C. J. Barrelet; C. M. Lieber, *Nano Lett.* **2004,** *4* (10), 1975-1979.
43. B. H. Le; S. Zhao; X. Liu; S. Y. Woo; G. A. Botton; Z. Mi, *Adv. Mater.* **2016,** *28* (38), 8446-8454.
44. S. Turkdogan; F. Fan; C. Z. Ning, *Adv. Fun. Mater.* **2016,** *26* (46), 8521-8526.
45. F. Fan; S. Turkdogan; Z. Liu; D. Shelhammer; C. Z. Ning, *Nat. Nanotechnol.* **2015,** *10* (9), 796-803.
46. Z. Yang; J. Xu; P. Wang; X. Zhuang; A. Pan; L. Tong, *Nano Lett.* **2011,** *11* (11), 5085-5089.
47. S. J. Kwon; H. M. Jeong; K. Jung; D. H. Ko; H. Ko; I. K. Han; G. T. Kim; J. G. Park, *ACS Nano* **2015,** *9* (5), 5486-5499.
48. C. H. Hsiao; S. J. Chang; S. B. Wang; S. P. Chang; Y. C. Cheng; T. C. Li; W. J. Lin; B. R. Huang, *J. Nanosci. Nanotech.* **2010,** *10* (2), 798-802.
49. S. J. Chang; C. H. Hsiao; S. B. Wang; Y. C. Cheng; T. C. Li; S. P. Chang; B. R. Huang; S. C. Hung, *Nanoscale Res. Lett.* **2009,** *4* (12), 1540-1546.
50. X. Chen; H. Li; Z. Qi; T. Yang; Y. Yang; X. Hu; X. Zhang; X. Zhu; X. Zhuang; W. Hu; A. Pan, *Nanotech.* **2016,** *27* (50), 505602.
51. K. Lee; B. M. Tienes; M. B. Wilker; K. J. Schnitzenbaumer; G. Dukovic, *Nano Lett.* **2012,** *12* (6), 3268-3272..
52. C. H. Chuang; Y. G. Lu; K. Lee; J. Ciston; G. Dukovic, *J. Am. Chem. Soc.* **2015,** *137* (20), 6452-6455.
53. K. Lee; Y. G. Lu; C. H. Chuang; J. Ciston; G. Dukovic, *J. Mater. Chem. A* **2016,** *4* (8), 2927-2935.
54. D. Wang; M. Zhang; H. Zhuang; X. Chen; X. Wang; X. Zheng; J. Yang, *Appl. Surf. Sci.* **2017,** *396*, 888-896.
55. J. Li; B. Liu; W. Yang; Y. Cho; X. Zhang; B. Dierre; T. Sekiguchi; A. Wu; X. Jiang, *Nanoscale* **2016,** *8* (6), 3694-3703.
56. K. Park; J. A. Lee; H. S. Im; C. S. Jung; H. S. Kim; J. Park; C. L. Lee, *Nano Lett.* **2014,** *14* (10), 5912-5919.
57. J. N. Hart; N. L. Allan, *Adv. Mater.* **2013,** *25* (21), 2989-2993.
58. W. Yang; B. Liu; B. Yang; J. Wang; T. Sekiguchi; S. Thorsten; X. Jiang, *Adv. Funct. Mater.* **2015,** *25* (17), 2543-2551.
59. Y. Wang; J. Xu; P. Ren; Q. Zhang; X. Zhuang; X. Zhu; Q. Wan; H. Zhou; W. Hu; A. Pan, *Phys. Chem. Chem. Phys.* **2013,** *15* (8), 2912-2916.
60. K. Maeda; T. Takata; M. Hara; N. Saito; Y. Inoue; H. Kobayashi; K. Domen, *J. Am. Chem. Soc.* **2005,** *127* (23), 8286-8287.
61. W. Q. Han; Z. Liu; H. G. Yu, *Appl. Phys. Lett.* **2010,** *96* (18), 183112.
62. Y. Li; L. Zhu; Y. Yang; H. Song; Z. Lou; Y. Guo; Z. Ye, *Small* **2015,** *11* (7), 871-876.
63. F. Gu; Z. Yang; H. Yu; J. Xu; P. Wang; L. Tong; A. Pan, *J. Am. Chem. Soc.* **2011,** *133* (7), 2037-2039.
64. M. Lopez-Ponce; A. Hierro; J. M. Ulloa; P. Lefebvre; E. Muñoz; S. Agouram; V. Muñoz-Sanjosé; K. Yamamoto; A. Nakamura; J. Temmyo, *Appl. Phys. Lett.* **2013,** *102* (14), 143103.

65. H. Zhou; M. Pozuelo; R. F. Hicks; S. Kodambaka, *J. Crys. Growth* **2011,** *319* (1), 25-30.
66. M. G. Kibria; F. A. Chowdhury; S. Zhao; B. AlOtaibi; M. L. Trudeau; H. Guo; Z. Mi, *Nat. Commun.* **2015,** *6*, 6797.
67. Y. N. Guo; H. Y. Xu; G. J. Auchterlonie; T. Burgess; H. J. Joyce; Q. Gao; H. H. Tan; C. Jagadish; H. B. Shu; X. S. Chen; W. Lu; Y. Kim; J. Zou, *Nano Lett.* **2013,** *13* (2), 643-650.
68. W. Du; X. Yang; H. Pan; X. Wang; H. Ji; S. Luo; X. Ji; Z. Wang; T. Yang, *Crys. Growth Des.* **2015,** *15* (5), 2413-2418.
69. C. Y. He; Q. A. Wu; X. Z. Wang; Y. L. Zhang; L. J. Yang; N. Liu; Y. Zhao; Y. N. Lu; Z. Hu, *ACS Nano* **2011,** *5* (2), 1291-1296.
70. X. H. Tang; B. L. Zhang; Z. Y. Yin, *Cryst. Eng. Comm.* **2013,** *15* (3), 604-608.
71. W. N. Du; X. G. Yang; H. Y. Pan; X. H. Ji; H. M. Ji; S. Luo; X. W. Zhang; Z. G. Wang; T. Yang, *Nano Lett.* **2016,** *16* (2), 877-882.
72. X. Yuan; P. Caroff; J. Wong-Leung; H. H. Tan; C. Jagadish, *Nanoscale* **2015,** *7* (11), 4995-5003.
73. A. Berg; M. Heurlin; S. Tsopanidis; M. E. Pistol; M. T. Borgstrom, *Nanotech.* **2017,** *28* (3), 035706.
74. Y. J. Hwang; C. H. Wu; C. Hahn; H. E. Jeong; P. Yang, *Nano Lett.* **2012,** *12* (3), 1678-1682.
75. Q. D. Zhuang; E. A. Anyebe; R. Chen; H. Liu; A. M. Sanchez; M. K. Rajpalke; T. D. Veal; Z. M. Wang; Y. Z. Huang; H. D. Sun, *Nano Lett.* **2015,** *15* (2), 1109-1116.
76. F. Glas; J. C. Harmand; G. Patriarche, *Phys. Rev. Lett.* **2010,** *104* (13), 135501.
77. L. Z. Liu; X. L. Wu; J. C. Shen; T. H. Li; F. Gao; P. K. Chu, *Chem. Commun.* **2010,** *46* (30), 5539-5541.
78. A. Patra; M. Chakraborty; A. Roy, *Nanoscale* **2016,** *8* (42), 18143-18149.
79. W. Metaferia; A. R. Persson; K. Mergenthaler; F. Yang; W. Zhang; A. Yartsev; R. Wallenberg; M. E. Pistol; K. Deppert; L. Samuelson; M. H. Magnusson, *Nano Lett.* **2016,** *16* (9), 5701-5707.
80. P. Ren; W. Hu; Q. Zhang; X. Zhu; X. Zhuang; L. Ma; X. Fan; H. Zhou; L. Liao; X. Duan; A. Pan, *Adv. Mater.* **2014,** *26* (44), 7444-7449.
81. R. Tenne; S. Pedetti; M. Kazes; S. Ithurria; L. Houben; B. Nadal; D. Oron; B. Dubertret, *Phys. Chem. Chem. Phys.* **2016,** *18* (22), 15295-15303.
82. A. M. Jagtap; V. Varade; B. Konkena; K. P. Ramesh; A. Chatterjee; A. Banerjee; N. B. Pendyala; K. S. R. Koteswara Rao, *J. Appl. Phys.* **2016,** *119* (7), 074306.
83. J. L. Wang; K. M. Chen; M. Gong; B. Xu; Q. Yang, *Nano Lett.* **2013,** *13* (9), 3996-4000.
84. G. X. Zhu; Z. Xu, *J. Am. Chem. Soc.* **2011,** *133* (1), 148-157.
85. W. Han; L. X. Yi; N. Zhao; A. W. Tang; M. Y. Gao; Z. Y. Tang, *J. Am. Chem. Soc.* **2008,** *130* (39), 13152-13161.
86. R. E. Bailey; S. Nie, *J. Am. Chem. Soc.* **2003,** *125* (23), 7100-7106.
87. Y. Zhou; Y. C. Li; H. Z. Zhong; J. H. Hou; Y. Q. Ding; C. H. Yang; Y. F. Li, *Nanotech.* **2006,** *17* (16), 4041-4047.
88. S. Lee; J. C. Flanagan; J. Kang; J. Kim; M. Shim; B. Park, *Sci Rep-Uk* **2016,** *6*.
89. B. Xing; W. Li; X. Wang; H. Dou; L. Wang; K. Sun; X. He; J. Han; H. Xiao; J. Miao; Y. Li, *J. Mater. Chem.* **2010,** *20* (27), 5664.
90. X. F. Li; Y. Cao; Y. R. Sui; J. H. Yang; Y. G. Yue; Q. Zhang; X. Y. Liu; M. Gao; J. H. Lang; X. Y. Li, *Superlatt. and Microstruc.* **2014,** *69*, 187-193.
91. L. J. Chen; C. R. Lee; Y. J. Chuang; Z. H. Wu; C. Chen, *Cryst. Eng. Comm.* **2015,** *17* (24), 4434-4438.
92. J. Du; X. Li; S. Wang; Y. Wu; X. Hao; C. Xu; X. Zhao, *J. Mater. Chem.* **2012,** *22* (22), 11390.

93. C. Y. Chen; G. Zhu; Y. Hu; J. W. Yu; J. Song; K. Y. Cheng; L. H. Peng; L. J. Chou; Z. L. Wang, *ACS Nano* **2012,** *6* (6), 5687-5692.
94. J. Cheng; D. Li; T. Cheng; B. Ren; G. Wang; J. Li, *J. Alloys Compd.* **2014,** *589*, 539-544.
95. X. Yan; X. Zhang; X. Ren; J. Li; X. Lv; Q. Wang; Y. Huang, *Appl. Phys. Lett.* **2012,** *101* (2), 023106.
96. H. Xu; Y. Liang; Z. Liu; X. Zhang; S. Hark, *Adv. Mater.* **2008,** *20* (17), 3294-3297.
97. M. G. Kibria; H. P. Nguyen; K. Cui; S. Zhao; D. Liu; H. Guo; M. L. Trudeau; S. Paradis; A. R. Hakima; Z. Mi, *ACS Nano* **2013,** *7* (9), 7886-7893.
98. N. Kornienko; D. D. Whitmore; Y. Yu; S. R. Leone; P. Yang, *ACS Nano* **2015,** *9* (4), 3951-3960.
99. A. T. M. G. Sarwar; B. J. May; R. C. Myers, *physica status solidi (a)* **2016,** *213* (4), 947-952.
100. A. Pan; R. Liu; M. Sun; C. Z. Ning, *ACS Nano* **2010,** *4* (2), 671-680.
101. H. S. Im; C. S. Jung; K. Park; D. M. Jang; Y. R. Lim; J. Park, *.J. Phys. Chem. C* **2014,** *118* (8), 4546-4552.
102. X. Duan; C. Wang; Z. Fan; G. Hao; L. Kou; U. Halim; H. Li; X. Wu; Y. Wang; J. Jiang; A. Pan; Y. Huang; R. Yu; X. Duan, *Nano Lett.* **2016,** *16* (1), 264-269.
103. A. Abdollahi; M. M. Golzan; K. Aghayar, *J. Alloys Compd.* **2016,** *675*, 86-93.
104. G. Mugny; J. Li; F. Triozon; Y.-M. Niquet; D. Rideau; C. Delerue, *Appl. Phys. Lett.* **2017,** *110* (5), 052102.
105. E. F. El-Wahidy; A. A. M. Farag; M. A. Rafea; N. Roushdy; O. El-Shazly, *Mater. Sci. Semicond. Processing* **2014,** *24*, 169-178.
106. Hajimu Sonomura; Tamotsu Uragaki; T. Miyauchi, *Jpn. J. Appl. Phys.* **1973,** *12* (7), 968-973.
107. S. Nakamura; T. Mukai; M. Senoh, *Appl. Phys. Lett.* **1994,** *64* (13), 1687-1689.
108. S. Zhao; S. M. Sadaf; S. Vanka; Y. Wang; R. Rashid; Z. Mi, *Appl. Phys. Lett.* **2016,** *109* (20), 201106.
109. Y. H. Ra; R. Wang; S. Y. Woo; M. Djavid; S. M. Sadaf; J. Lee; G. A. Botton; Z. Mi, *Nano Lett.* **2016,** *16* (7), 4608-4615.
110. Y.-H. Ra; R. Navamathavan; H. I. Yoo; C. R. Lee, *Nano Lett.* **2014,** *14* (3), 1537-1545.
111. H. P. T. Nguyen; K. Cui; S. Zhang; M. Djavid; A. Korinek; G. A. Botton; Z. Mi, *Nano Lett.* **2012,** *12* (3), 1317-1323.
112. M. R. Philip; D. D. Choudhary; M. Djavid; M. N. Bhuyian; J. Piao; T. T. Pham; D. Misra; H. P. T. Nguyen, *Journal of Vacuum Science & Technology B, Nanotechnology and Microelectronics: Materials, Processing, Measurement, and Phenomena* **2017,** *35* (2), 02B108.
113. C. B. Siao; K. W. Wang; H. S. Chen; Y. S. Su; S. R. Chung, *Opt. Mater. Express* **2016,** *6* (3), 749.
114. H. Zou; M. Liu; D. Zhou; X. Zhang; Y. Liu; B. Yang; H. Zhang, *J. Phys. Chem. C* **2017,** *121* (9), 5313-5323.
115. C. C. Shen; W. L. Tseng, *Inorg. Chem.* **2009,** *48* (18), 8689-8694..
116. C. Li; J. B. Wright; S. Liu; P. Lu; J. J. Figiel; B. Leung; W. W. Chow; I. Brener; D. D. Koleske; T. S. Luk; D. F. Feezell; S. R. J. Brueck; G. T. Wang, *Nano Lett.* **2017,** *17* (2), 1049-1055.
117. F. Fan; Z. Liu; L. Yin; P. L. Nichols; H. Ning; S. Turkdogan; C. Z. Ning, *Semicond. Sci. Tech.* **2013,** *28* (6), 065005.
118. D. Wu; Y. Chang; Z. Lou; T. Xu; J. Xu; Z. Shi; Y. Tian; X. Li, *J. Alloys Compd.* **2017,** *708*, 623-627.

119. P. Guo; J. Xu; K. Gong; X. Shen; Y. Lu; Y. Qiu; J. Xu; Z. Zou; C. Wang; H. Yan; Y. Luo; A. Pan; H. Zhang; J. C. Ho; K. M. Yu, *ACS Nano* **2016,** *10* (9), 8474-8481.
120. H. Tan; C. Fan; L. Ma; X. Zhang; P. Fan; Y. Yang; W. Hu; H. Zhou; X. Zhuang; X. Zhu; A. Pan, *Nano-Micro Letters* **2015,** *8* (1), 29-35.
121. B. M. Wong; F. o. Léonard; Q. Li; G. T. Wang, *Nano Lett.* **2011,** *11* (8), 3074-3079.
122. J. J. Hou; F. Wang; N. Han; F. Xiu; S. Yip; M. Fang; H. Lin; T. F. Hung; J. C. Ho, *ACS Nano* **2012,** *6* (10), 9320-9325.
123. Y. Li; J. Xiang; F. Qian; S. Gradečak; Y. Wu; H. Yan; D. A. Blom; C. M. Lieber, *Nano Lett.* **2006,** *6* (7), 1468-1473.
124. A. V. Thathachary; N. Agrawal; L. Liu; S. Datta, *Nano Lett.* **2014,** *14* (2), 626-633.
125. B. I. MacDonald; A. Martucci; S. Rubanov; S. E. Watkins; P. Mulvaney; J. J. Jasieniak, *ACS Nano* **2012,** *6* (7), 5995-6004.
126. Z. Pan; K. Zhao; J. Wang; H. Zhang; Y. Feng; X. Zhong, *ACS Nano* **2013,** *7* (6), 5215-5222.
127. J. Yang; J. Wang; K. Zhao; T. Izuishi; Y. Li; Q. Shen; X. Zhong, *J. Phys. Chem. C* **2015,** *119* (52), 28800-28808.
128. G. Wang; H. Wei; Y. Luo; H. Wu; D. Li; X. Zhong; Q. Meng, *J. Power Sour.* **2016,** *302*, 266-273.
129. J. Kou; Z. Li; Y. Guo; J. Gao; M. Yang; Z. Zou, *J. Mol. Catal. A: Chem.* **2010,** *325* (1-2), 48-54.
130. S. K. Pandey; S. Pandey; A. C. Pandey; G. K. Mehrotra, *Appl. Phys. Lett.* **2013,** *102* (23), 233110.
131. T. Hisatomi; J. Kubota; K. Domen, *Chem. Soc. Rev.* **2014,** *43* (22), 7520-35.
132. Q. Li; H. Meng; P. Zhou; Y. Zheng; J. Wang; J. Yu; J. Gong, *ACS Catalysis* **2013,** *3* (5), 882-889.
133. M. Liu; Y. Chen; J. Su; J. Shi; X. Wang; L. Guo, *Nat. Ener.* **2016,** *1*, 16151.
134. C. Hahn; M. A. Fardy; C. Nguyen; M. Natera-Comte; S. C. Andrews; P. Yang, *Israel Journal of Chemistry* **2012,** *52* (11-12), 1111-1117.
135. K. Maeda; K. Teramura; K. Domen, *J. Catal.* **2008,** *254* (2), 198-204.
136. T. Ohno; L. Bai; T. Hisatomi; K. Maeda; K. Domen, *J. Am. Chem. Soc.* **2012,** *134* (19), 8254-8259.
137. T. K. Sung; J. H. Kang; D. M. Jang; Y. Myung; G. B. Jung; H. S. Kim; C. S. Jung; Y. J. Cho; J. Park; C. L. Lee, *J. Mater. Chem.* **2011,** *21* (12), 4553.
138. J. M. Amatya; J. A. Floro, *Appl. Phys. Lett.* **2016,** *109* (19), 193112.
139. C. J. Kim; J. E. Yang; H. S. Lee; H. M. Jang; M. H. Jo; W. H. Park; Z. H. Kim; S. Maeng, *Appl. Phys. Lett.* **2007,** *91* (3).
140. M. Belloeil; B. Gayral; B. Daudin, *Nano Lett.* **2016,** *16* (2), 960-966.
141. F. Qian; S. Gradečak; Y. Li; C. Y. Wen; C. M. Lieber, *Nano Lett.* **2005,** *5* (11), 2287-2291.
142. A. T. Sarwar; S. D. Carnevale; F. Yang; T. F. Kent; J. J. Jamison; D. W. McComb; R. C. Myers, *Small* **2015,** *11* (40), 5402-5408.
143. J. C. Shin; K. H. Kim; K. J. Yu; H. Hu; L. Yin; C. Z. Ning; J. A. Rogers; J. M. Zuo; X. Li, *Nano Lett.* **2011,** *11* (11), 4831-4838.
144. G. Otnes; M. Heurlin; X. Zeng; M. T. Borgstrom, *Nano Lett.* **2017,** *17* (2), 702-707.
145. A. Berg; P. Caroff; N. Shahid; M. N. Lockrey; X. M. Yuan; M. T. Borgstrom; H. H. Tan; C. Jagadish, *Nano Res.* **2017,** *10* (2), 672-682.
146. Y. Wang; J. Xu; P. Ren; X. Zhuang; H. Zhou; Q. Zhang; X. Zhu; A. Pan, *Mater. Lett.* **2013,** *105*, 90-94.
147. H. Lee; P. H. Holloway; H. Yang, *J. Chem. Phys.* **2006,** *125* (16).
148. Z. Liu; X. T. Zhang; S. K. Hark, *Crys. Growth & Des.* **2009,** *9* (2), 803-806.

149. S. J. Chang; C. H. Hsiao; S. C. Hung; S. H. Chih; B. W. Lan; S. B. Wang; S. P. Chang; Y. C. Cheng; T. C. Li; B. R. Huang, *J. Electrochem. Soc.* **2010,** *157* (1), K1.
150. F. Xu; B. Xue; F. Wang; A. Dong, *Chem. Mater.* **2015,** *27* (3), 1140-1146.
151. V. Lesnyak; A. Dubavik; A. Plotnikov; N. Gaponik; A. Eychmuller, *Chem. Commun.* **2010,** *46* (6), 886-888.
152. L. J. Chen; J. H. Dai, *Opt. Mater.* **2017,** *64*, 356-360.
153. J. Sun; Y. M. Chen; Z. N. Xu; Q. S. Chen; G. E. Wang; M. J. Zhang; G. Lu; K. C. Wu; G. C. Guo, *Cryst. Eng. Comm.* **2014,** *16* (30), 6823-6826.
154. T. Pons; N. Lequeux; B. Mahler; S. Sasnouski; A. Fragola; B. Dubertret, *Chem. Mater.* **2009,** *21* (8), 1418-1424.
155. Y. C. Li; H. Z. Zhong; R. Li; Y. Zhou; C. H. Yang; Y. F. Li, *Adv. Fun. Mater.* **2006,** *16* (13), 1705-1716.
156. C. Ngo; H. Zhou; M. Mecklenburg; M. Pozuelo; B. C. Regan; Q. F. Xiao; V. B. Shenoy; R. F. Hicks; S. Kodambaka, *J. Crys. Growth* **2011,** *336* (1), 14-19.
157. D. Ren; J. Huh; D. L. Dheeraj; H. Weman; B.-O. Fimland, *Appl. Phys. Lett.* **2016,** *109* (24), 243102.
158. L. Li; D. Pan; Y. Xue; X. Wang; M. Lin; D. Su; Q. Zhang; X. Yu; H. So; D. Wei; B. Sun; P. Tan; A. Pan; J. Zhao, *Nano Lett.* **2017,** *17* (2), 622-630.
159. D. Ren; D. L. Dheeraj; C. Jin; J. S. Nilsen; J. Huh; J. F. Reinertsen; A. M. Munshi; A. Gustafsson; A. T. van Helvoort; H. Weman; B. O. Fimland, *Nano Lett.* **2016,** *16* (2), 1201-1209.
160. J. C. Harmand; F. Jabeen; L. Liu; G. Patriarche; K. Gauthron; P. Senellart; D. Elvira; A. Beveratos, *J. Crys. Growth* **2013,** *378*, 519-523.
161. Y. Kuwahara; H. Oyanagi; R. Shioda; Y. Takeda; H. Kamei; M. Aono, *J. Appl. Phys.* **1997,** *82* (1), 214-218.
162. L. Zhang; L. Fan; G. N. Panin; T. W. Kang; K. Zheng, *Mater. Lett.* **2015,** *148*, 55-57.
163. E. Kowsari; M. R. Ghezelbash, *Mater. Lett.* **2011,** *65* (23-24), 3371-3373.
164. S. Taniguchi; M. Green; T. Lim, *J. Am. Chem. Soc.* **2011,** *133* (10), 3328-3331.
165. L. L. Pang; H. J. Cui; Y. Liu; W. Y. Zhong, *J. Lumin.* **2016,** *173*, 274-278.
166. S. G. Ghalamestani; M. Ek; M. Ghasemi; P. Caroff; J. Johansson; K. A. Dick, *Nanoscale* **2014,** *6* (2), 1086-1092.
167. Y. Zhang; M. Aagesen; J. V. Holm; H. I. Jorgensen; J. Wu; H. Liu, *Nano Lett.* **2013,** *13* (8), 3897-902. DOI 10.1021/nl401981u.
168. W. Sun; Y. Guo; H. Xu; Q. Gao; H. Hoe Tan; C. Jagadish; J. Zou, *Appl. Phys. Lett.* **2013,** *103* (22), 223104. DOI 10.1063/1.4834377.
169. Z. Deng; H. Yan; Y. Liu, *J. Am. Chem. Soc.* **2009,** *131* (49), 17744-17745. .

TOC Figure

Semiconductor solid-solution nanostructures: synthesis, property tailoring and applications

Baodan Liu,[1,] Jing Li,[1] Wenjin Yang,[1] Xinglai Zhang,[1] Xin jiang[1] and Yoshio Bando[2]*